Dynamics of periodic ribbed plates with inner resonance Analytical homogenized model and dispersion features

Pascal Fossat, Claude Boutin, Mohamed Ichchou

Dynamics of periodic ribbed plates with inner resonance: Analytical homogenized model and dispersion features

P. Fossat [a,b], C. Boutin [a,*], M. Ichchou [b]

[a] *École Nationale des Travaux Publics de l'État, Université de Lyon, LGCB, UMR-CNRS 5513, Rue Maurice Audin, Vaulx-en-Velin 69518, France*
[b] *École Centrale de Lyon, LTDS, UMR-CNRS 5513, 36 Avenue Guy de Collongue, Ecully 69134, France*

The dynamic behavior of a periodic ribbed plate with local resonance is investigated. The behavior of the cell made of a beam clamped along a plate edge analyzed through multi-scale asymptotic method enables to derive the governing equations of the effective mechanical behavior. This approach allows obtaining a full homogenized analytical model that provides a relevant representation of the flexural and torsional mechanisms at both global and local scales. The complex dynamic behavior is shown to encompass several mechanisms associated with enriched kinematics. Two types of flexural and torsional waves are evidenced and governed by two distinct differential equations that describes (i) waves where both beam and plate moves, and (ii) guided waves where the plate only is set in motion. The inner resonance of the plate induces unconventional dispersion features, with singularities associated either with the symmetric eigenmodes for the bending waves or the antisymmetric modes for the torsional waves. The guided waves are alternatively related to the symmetric and antisymmetric modes of the bended plate and are propagative above the corresponding eigenfrequencies. The predictions of the homogenized model are successfully compared to numerical calculations conducted using Wave Finite Element based methods, for two realistic examples of ribbed plates. The study provides design rules to tailor ribbed plate panels having specific atypical features in a given frequency range.

1. Introduction

Composite panels with optimized vibroacoustic features practically lead to highly heterogeneous structures made of different components, often periodically distributed *e.g.* honeycombs, sandwich panels, ribbed plates, beam truss/slats. Such structures are widely used in automotive and aerospace industry, civil engineering, where a planar structure may be stiffened by a periodic layout of beams. The prediction of their dynamic behavior is then of interest from theoretical and practical point of view.

The classical plates models are well suited for homogeneous structures or moderately heterogeneous structures. However difficulties appear when attempting to extend classical theories to composite structures with significantly contrasted properties. For instance, when considering ribbed plates, in the case where the stiffeners present similar rigidity and size characteristics than that of the plate, then the global behavior will be that of a classical anisotropic plate. Conversely, if the stiffeners are much stiffer than the plate, the global behavior of will be that of a set of parallel beams. In intermediary situations a specific beam/plate coupled behavior should exist. The present paper focuses on this specific situation in dynamic regime, in which the beam/plate contrasts induce inner resonance phenomena.

Several semi-analytical and numerical models have been developed to study the dynamics of stiffened plates. The common ribbed plate model given by an equivalent orthotropic plate with mean mass density and effective stiffnesses applies in quasi-statics but fails to describe the specific features of the plate dynamics (Ichchou et al., 2008a). In dynamics, a reference study on significantly heterogeneous uni-directionally ribbed panels has been conducted by Fahy and Lindqvist (1976) following the assumption that a pure flexural motion exists in the plates and pure flexural/torsional motion exist in the ribs (Ungar, 1961). This approach does not provides a plate model but yields the dispersion equations analytically, that can be solved numerically, and it has been validated experimentally that this method predicts reliably the dispersion properties of waves in uni-directionally ribbed plate (Ichchou et al., 2008b). In the same spirit, a numerical model based on a modal expansion technique that takes into account the moment and force coupling between the ribs and the plate is proposed by Mejdi and Atalla (2010) to compute the mechanical and acoustical frequency response of orthogonally ribbed plate. At the

* Corresponding author.
E-mail address: claude.boutin@entpe.fr (C. Boutin).

same time, numerical approaches based on the Floquet–Bloch theory has been developed to obtain the propagation features of periodic ribbed plates. This method called WFEM (Mead, 1973; Waki et al., 2009), has been used by Ichchou et al. (2008b) to recover (i) the results of the Fahy's approach (Fahy and Lindqvist, 1976), and (ii) experimental dispersion curves. Recently, energetic method based on a semi-analytical variational formulation has also been considered (Trévisan et al., 2016). Numerous other methods such as the plane-wave expansion method, finite elements based methods, transfer matrix method, are reviewed in Hussein et al. (2014) in the framework of mechanical metamaterials.

The above mentioned studies provide accurate numerical results for given designs. However, these formulations do not enable to identify the underlying model that arises from the physics involved within the cell. Moreover, the numerical modeling of large structures with high mechanical and geometrical contrasts are facing to ill-conditioned problems (Waki et al., 2009) that leads to discretization errors (Mace et al., 2005) or aliasing effect (Ichchou et al., 2007).

Model reduction through periodic homogenization method (Sanchez-Palencia, 1980; Auriault et al., 2009) is a way to overcome these issues. Precisely, this technique allows to up-scale the physics at microscale into a macroscopic model, in which the effective parameters are fully determined from the periodic cell. The relevancy of the up-scaled description is insured by taking into account the key physical phenomena at local and global scales. The strategy consists in considering domains made of a large number of periods, and phenomena evolving at a macroscopic length characterized by the dimension L significantly larger than the size l of the cell. Hence, the principle is to perform the asymptotic expansions of the fields involved in the problem in terms of the dimensionless scale parameter $\epsilon = l/L$. Numerous usual composites have a periodic configuration with a period much smaller than their global dimensions therefore asymptotic homogenization appears to be an appropriate method for analysis.

A decisive advantage of this approach is to build-up the macroscopic model without making a priori conjectures on the model to be found. In particular, it enables to handle the case of highly contrasted composites or structures and to point out their unconventional behavior as higher-order gradient generalized media (Soubestre and Boutin, 2012), or inner resonance media. For example, in 3D composites, due to the inner resonance of soft inclusions, the effective mass becomes tensorial and takes negative values over bands centered around the inner resonance frequencies (Auriault and Bonnet, 1985; Boutin, 1996; Auriault and Boutin, 2012). Such an effect can also appears in reticulated media (Chesnais et al., 2012).

Asymptotic methods has been extensively applied to develop plate theories considering homogeneous plates, (Trabucho and Viaño, 1996; Ciarlet, 1997), plates made of periodic composite (Caillerie, 1984), thin homogeneous plates with rapidly varying thickness (Kohn and Vogelius, 1984). One may refer to Lewiński and Telega (2000), Altenbach et al. (2010), and Kalamkarov et al. (2009) for comprehensive reviews on plates and shells. The aspect of highly contrasted constituents has been handled for laminates (Berdichevsky, 2010; Viverge et al., 2016), however up to our knowledge, the case of highly contrasted ribbed plate is not yet addressed by homogenization in the literature.

The purpose of the present work is to derive asymptotic homogenized models for periodic uni-directionally ribbed plates with strong mechanical contrast as illustrated in Fig. 1. This work uses the ideas of beam/plate coupling (Fahy and Lindqvist, 1976), homogenization of inner resonance media (Auriault and Bonnet, 1985), together with asymptotic modeling of beams and plates (Trabucho and Viaño, 1996; Ciarlet, 1997), and numerical procedure WFEM (Ichchou et al., 2008b). The paper is divided into six sections. Section 2 describes the physical mechanisms, assuming that the size of the cell is short with respect to the wavelength. From the dimensional analysis, the possible contrasts suitable for the existence of inner resonance are discussed. Section 3 presents the asymptotic homogenization procedure and details the beam/plate coupling. Sections 4 and 5 focus respectively on the flexural and torsional behaviors. One derives an homogenized analytical model encompasses the mechanisms at both global and local scales. The complex dynamic behavior is shown to involve enriched kinematics. Actually, two types of flexural and torsional waves are evidenced, governed by two distinct differential equations that describes (i) waves where both beams and plates move, and (ii) guided waves where the plates only are set in motion. It is shown that the inner resonance of the plate induces unconventional dispersion features with singularities associated either with the symmetric eigenmodes for the bending waves or the antisymmetric modes for the torsional wave. The guided waves are alternatively related to the symmetric and antisymmetric modes of the bended plate and are propagative above the corresponding eigenfrequencies. Finally, in Section 6, the predictions of the homogenized model are successfully compared to numerical calculations conducted using WFEM based method, for two realistic examples of ribbed plates. By principle, the WFE method predicts reliably the dispersion properties of waves propagating in ribbed plates but the obtained dispersion diagram is somehow difficult to understand. The proposed model brings a physical interpretation by analyzing the kinematics and deriving explicit dispersion equations associated with the various branches. In conclusion, it is stressed that the study yields design rules to tailor ribbed plate panels having atypical features in a given frequency range.

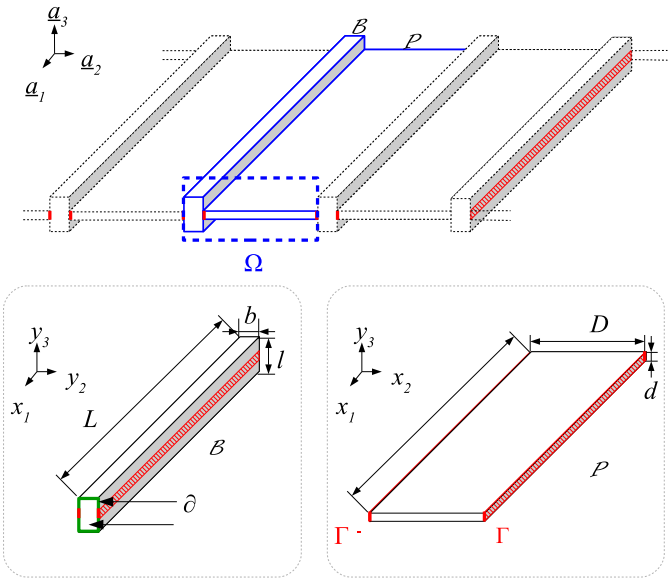

Fig. 1. Periodic ribbed plate under study with constitutive cell Ω and local coordinates associated with the beam $\mathcal{B}$ and the plate $\mathcal{P}$ clamped on their interfaces $\Gamma_b^{\pm}$, $\Gamma_p^{\pm}$.

2. Physical analysis

2.1. Studied structure

The periodic ribbed plate under study is depicted in Fig. 1 and comprises identical plate elements (denoted $\mathcal{P}$) rigidly connected to regularly spaced identical straight beams (denoted $\mathcal{B}$). Thus, the period Ω consists in a beam and a plate element, i. e. $\Omega = \mathcal{B} \cup \mathcal{P}$, both being assumed homogeneous. The beam $\mathcal{B}$ is characterized by its length L, thickness l and width b, with $b = O(l)$. The plate $\mathcal{P}$ is

of length L, thickness d, width D. The constituting material of $\mathcal{B}$ and $\mathcal{P}$ is isotropic elastic, having a Young's modulus E_b, Poisson's ratio ν_b, and density ρ_b for the beam, and respectively (E_p, ν_p, ρ_p) for the plate.

The boundary of the beam section S_b is denoted ∂S_b and $\Gamma_b = \Gamma_b^- \cup \Gamma_b^+$ is the beam/plate interface (where $^+$ and $^-$ refer to the normal orientation along $\underline{a}_2$ and $-\underline{a}_2$ respectively). Similarly the plate/beam interface is $\Gamma_p = \Gamma_p^- \cup \Gamma_p^+$. Hence, the interface of Ω with the two adjacent period is $\Gamma_\Omega = \Gamma_b^- \cup \Gamma_p^+$, and the inner interface is Γ_b^+ that coincides with Γ_p^- with opposite normal orientation.

From the geometry of the beam $\mathcal{B}$ and of the plate $\mathcal{P}$ we are lead to identify three small parameters related to the beam, to the plate and to the ribbed plate:

- *for the beam* $\mathcal{B}$, ϵ_b is the inverse of its slenderness $\epsilon_b = l/L \ll 1$
- *for the plate* $\mathcal{P}$, ϵ_p is the inverse of its flatness $\epsilon_p = d/D \ll 1$
- *for the ribbed plate*, ε is the inverse of the Ω-cell's slenderness, i.e., the ratio between the plate width D and L, that is $\varepsilon = D/L \ll 1$

The contrasts of mechanical properties of the constituting materials of the beam $\mathcal{B}$ and plate $\mathcal{P}$ are specified by E_p/E_b and ρ_b/ρ_p. To sum up, the ribbed plate is characterized by the set of five dimensionless parameters, $\{\epsilon_b, \epsilon_p, \varepsilon, E_p/E_b, \rho_b/\rho_p\}$.

The model is developed considering harmonic regimes at angular frequency ω, and, by linearity, the time dependence $\exp(i\omega t)$ is omitted hereinafter.

2.2. Physical insight into the inner resonance in ribbed plates

The present analysis of ribbed plates is inspired from the study of inner resonance in periodic elastic composites as developed in Auriault and Bonnet (1985) and Auriault and Boutin (2012). The inner resonance corresponds to situations where dynamic phenomena co-exist at both the micro-scale of the period and the macro-scale of the structure. It has been shown that such a specific regime, named 'co-dynamics' regime, occurs only in heterogeneous materials with sufficiently contrasted properties. For instance, in a bi-composite, a stiff and connected constituent conveys the long wavelength – and then undergoes a local quasi-static regime – while, at the same frequency, the other constituent experiences a local dynamic regime. This description highlights the two main distinctive features of the inner resonance regime, that are (i) the co-existence at the same frequency of long and short wavelengths in the different constituents, and, as a corollary, (ii) a specific static-dynamic regime at the period scale that generates an non-conventional inhomogeneous kinematics in the sense that the displacements of the two constituents differ at the leading order. These peculiarities clearly indicate that both constituents play a different role and therefore that their coupling is not symmetric. This asymmetry implies that one constituent is forcing and the other one is forced. In actual fact, the forcing constituent is the stiff one that carries the long wavelength while the forced one experiences short waves inducing the local resonance.

In ribbed plates undergoing out-of-plane vibrations the same principles apply. The stiff beam plays the role of the forcing constituent that conveys the large wavelength, while the soft plate acts as the forced constituent that experiences the local resonance. Conducting a dimensional analysis based on these basic ideas enables to express, in terms of geometrical and mechanical parameters, the conditions to reach a co-dynamic regime. However they are no so straightforward as in the case of the elastic composites, because (i) the different small parameters related to the beam and plate geometry, and (ii) the different orientations of the wave in the beam and in the plate element as explained hereafter.

2.2.1. The "co-dynamic" condition

A first requirement for the appearance of inner resonances is obtained by expressing the "co-dynamic" condition. The dynamic equation describing the flexural motion of the beam $\mathcal{B}$ alone (i.e. not connected to the plate) along its axis $\underline{a}_1$ reads (see axis of Fig. 1)

$$E_b I_b \partial_{x_1}^4 U = \Lambda_b \omega^2 U$$

where U is the transverse displacement along $\underline{a}_3$, $I_b = bl^3/12$ is the moment of inertia of the beam around $\underline{a}_2$, $S_b = bl$ is the beam section, and $\Lambda_b = \rho_b S_b$ its lineic mass. Thus, the reduced bending wavelength (i.e. the wavelength divided by 2π) $\mathcal{L}_\omega$ is given by:

$$\mathcal{L}_\omega^4 = O\Big(\frac{E_b I_b}{\Lambda_b \omega^2}\Big)$$

The fundamental resonance ω_b of a beam of length L is such that $\mathcal{L}_{\omega_b} = L$ and consequently:

$$\omega_b^2 = O\Big(\frac{E_b I_b}{\Lambda_b L^4}\Big)$$

As for the plate $\mathcal{P}$, its local resonance happens within the period, which in our case is defined along $\underline{a}_2$ and is of length D. Consequently, we have to consider the one-dimensional dynamic equation that describe the flexural motion of the plate $\mathcal{P}$ along the $\underline{a}_2$ axis. It reads

$$E_p' I_p \partial_{x_2}^4 w = \Lambda_p \omega^2 w$$

where w is the out-of-plane displacement along $\underline{a}_3$, $E_p' I_p$ is the flexural stiffness, with $E_p' = E_p/(1-\nu_p^2)$ the "plate modulus", $I_p = d^3/12$ the moment of inertia around the $\underline{a}_1$ axis, and $\Lambda_p = \rho_p d$ the surface mass. Hence, the fundamental resonance frequency of a plate of length D is estimated as:

$$\omega_p^2 = O\Big(\frac{E_p' I_p}{\Lambda_p D^4}\Big)$$

Considering the situation of inner resonance where the beam and plate fundamental resonances are of the same order, i.e., $\omega_b/\omega_p = O(1)$, we are lead to the following requirement

$$\frac{E_b l^2}{\rho_b L^4} = O\Big(\frac{E_p' d^2}{\rho_p D^4}\Big) \qquad \text{i.e.} \qquad \frac{E_b \rho_p}{E_p' \rho_b} = O\Big(\frac{d^2}{l^2}\frac{L^4}{D^4}\Big) = O\Big(\frac{\epsilon_p^2}{\epsilon_b^2 \varepsilon^2}\Big) \tag{1}$$

Note that a similar relation (adjusted by numerical factors) would be obtained by considering higher modes instead of fundamental modes. Remark also that for infinite plates the "co-dynamic" condition implies that at frequency $O(\omega_p)$, the beam $\mathcal{B}$ is in dynamic regime so that the characteristic lengths of the motions in the beam is in that case $\mathcal{L}_{\omega_p}^4 = O\Big(\frac{E_b I_b}{E_p' I_p}\frac{\Lambda_p}{\Lambda_b} D^4\Big)$.

2.2.2. Condition of asymmetric coupling

As above stated, the inner resonance necessarily involves an inhomogeneous kinematics associated with an asymmetric beam/plate coupling. Indeed, a symmetric coupling would induces a similar regime in both elements. Therefore they would behave globally according to an homogeneous kinematic that avoids the inner resonance. We consider ribbed plates such that the stiff beam acts as the forcing - or driving - system that imposes its displacement to the forced – or driven – plate. In response, the forces exerted by the plate on the beam acts as a surface source that loads the beam. In other words, considering the transverse balance, i.e. along $\underline{a}_3$, of the beam loaded by the plate, the asymmetric beam/plate coupling imposes that

$$\partial_{x_1} T_b = O(T_p) \tag{2}$$

where T_b denotes the transverse shear force (unit kN) in the beam $\mathcal{B}$ and T_p the transverse linear shear force in the plate $\mathcal{P}$ (unit kN/m). Let us specify the case where fundamental resonances of the beam and plate are of the same order.

Since the beam is the forcing system, its constitutive equation remains unchanged by the external loading. Hence, following the Euler behavior of slender beam in dynamic regime, T_b and $\partial_{x_1} T_b$ can be assessed as

$$T_b = O(E_b I_b \partial^3_{x_1} U) = O\left(E_b \frac{bl^3}{12}\frac{U}{L^3}\right) \quad ; \quad \partial_{x_1} T_b = O\left(E_b \frac{bl^3}{12}\frac{U}{L^4}\right)$$

As the plate is vibrating along the $\underline{a}_2$-direction of length D, according to the Love–Kirchhoff behavior of thin plates, T_p is estimated as:

$$T_p = O(E'_p I_p \partial^3_{x_2} w) = O\left(E'_p \frac{d^3}{12}\frac{w}{D^3}\right)$$

The plate and beam displacements are identical at their junction, and consequently we have $w = O(U)$. Thus, from (2) and recalling that ,$b = O(l)$, one deduces the following requirement

$$O\left(E_b \epsilon_b^4\right) = O\left(E_p \epsilon_p^3\right) \tag{3}$$

2.2.3. Possible designs suitable for inner resonant ribbed plates

Conditions (1) and (3) can be achieved for different scaling of the five dimensionless parameters characterizing the ribbed plate. Let us examine two combinations of parameters that offer the possibility of simple practical realizations.

Consider a ribbed plate such that the flatness d/D of the plate is of the same order as the slenderness l/L of the beam. With these assumptions $\epsilon_b = l/L = d/D = \epsilon_p = \epsilon$ and, in turn, $\varepsilon = O(D/L) = O(d/l)$. Thus, requirements (1) and (3) imposes respectively that

$$\frac{E'_p \rho_b}{E_b \rho_p} = \frac{D^2}{L^2} = O(\varepsilon^2) \quad ; \quad \frac{E'_p}{E_b} = l/L = d/D = O(\epsilon) \tag{4}$$

which means that the plate modulus is much smaller than that of the beam and that the density ratio ρ_b/ρ_p is of the order of $O(\epsilon/\varepsilon^2)$. Relations (4) correspond to an heterogeneous ribbed plate made of a narrow and thin plate in comparison with the beam length and thickness, respectively. By construction, when relations (4) are satisfied, an inner resonance situation is expected in the frequency range around the common fundamental frequency of the plate and the beam.

It is also of interest to consider the case where the plate and beam materials are identical ($E_p = E_b,\ \rho_p = \rho_b$). In that case, the requirements (1) and (3) yields

$$\frac{d^2}{l^2}\frac{L^4}{D^4} = \frac{\epsilon_p^2}{\epsilon_b^2 \varepsilon^2} = O(1) \quad ; \quad \frac{l^4}{L^4}\frac{D^3}{d^3} = \frac{\epsilon_b^4}{\epsilon_p^3} = O(1) \tag{5}$$

from which one deduces that

$$\varepsilon = D/L = O(\sqrt{d/l}) \ll 1 \quad \text{and} \quad dD = O(l^2)$$

The two above relations defines the geometry of inner resonant ribbed plates made of a single material with given values of the thicknesses d and l.

Note that, in both designs, the bending deformability of plate is significantly larger than that of the beam due to smaller thickness and/or Young modulus (in the first situation $d/l = O(\varepsilon)$; $E_p/E_b = O(\varepsilon^2)$; and in the second one $d/l = O(\varepsilon^2)$; $E_p/E_b = 1$). This is consistent with the analysis in terms of forcing beam and forced plate.

2.3. Conduct of the homogenization process

The homogenization method is well suited to handle systems with strong contrasts of properties, and in which physical variables that exhibit slow variations interact with other variables that exhibit fast variations. In general, these features lead to ill-conditioned numerical formulation. However, owing to the asymptotic approach, the two sets of variables can be dissociated which makes the resolution tractable. This enables to determine an effective model whose parameters are directly inherited from the microstructure. Let us focus on how the homogenization method will be applied in the present case.

The homogenization method is based on the key assumption of scale separation (wavelength much larger that the period size). This is explicitly formulated through the asymptotic expansions of the variables that also accounts from the scaling issued from the dimensional analysis. The usual implementation of this method leads to solve the local problems by considering the period as a whole, (Sanchez-Palencia, 1980; Auriault et al., 2009). In the present case, the asymmetric coupling between the cell constituents means that the driving beam imposes its displacement to the plate and in turn is subjected to the stresses exerted by the plate. Reciprocally, the driven plate is subjected to the beam displacement and imposes its stresses to the beam. Consequently, the usual procedure can be tailored and decomposed into the three following steps:

1. derivation of the beam model based on the scale ratio ϵ_b, (Section 3.1.1)
2. derivation of the plate model based on the scale ratio ϵ_p, (Section 3.1.2)
3. derivation of the ribbed plate model based on the scale ratio ε. (Section 3.2).

Notice that conveniently the scale ratio ϵ_b and ε are defined by considering the beam length L as the characteristic size of the variations at large scale. This is consistent with the analysis of the fundamental and/or few first modes. However, when dealing with higher frequencies, the characteristic size would be the reduced bending wavelength $\mathcal{L}_{\omega_p}$ instead of L.

3. Homogenization of the flexural behavior of ribbed plates with inner resonance

3.1. Asymptotic bending models of beams and plates

We focus here on the steps 1 and 2 above indicated. The elaboration of the models is a direct application of the asymptotic methods dedicated to the formulation of beam or plate theory from (i) the 3D isotropic elasticity of the media, (ii) the slenderness or the flatness condition and (iii) the specific loading by surface and/or body forces, (Trabucho and Viaño, 1996; Ciarlet, 1997), (see also papers dedicated to contrasted composites involving beam or plates (Soubestre and Boutin, 2012; Viverge et al., 2016)). Hence, for conciseness, the derivation of the beam and plate models will not be detailed here since they correspond to classical Euler beam and Love–Kirchhoff plate. However, to illustrate the asymptotic procedure, the main steps are reported in Appendix A (a similar approach would lead to the plate model).

Nevertheless, in both models it is necessary to pay attention to the orders of magnitude of the physical variables (displacements, strains, stresses) which are the crucial issue for the consistency of the matching conditions. Indeed the latter have to be expressed on the beam/plate interface through the expanded variables in beam and plate.

Let us also underline that, in addition to the fact that the small parameters of the beam and plate can differ, the problem geometry is such that x_1 (respectively y_3) is a macroscopic (respectively microscopic) variable for both the beam and the plate, while the status of spatial variable associated with the $\underline{a}_2$ axis changes from microscopic in the beam to macroscopic for the plate.

3.1.1. Asymptotic model of the beam $\mathcal{B}$

The straight and homogeneous beam $\mathcal{B}$ satisfies the slenderness criterion $\epsilon_b = l/L \ll 1$. The reference orthonormal frame $(\underline{a}_1, \underline{a}_2, \underline{a}_3)$ shown in Fig. 1 is orientated following the main axes of inertia and its origin matches with the center of mass of the section. The approach is based on the fact that the beam geometry differentiates the axial and transverse directions ; it also suggests that the phenomena vary along the axis according to L and within the section according to l. This has three main consequences.

First, the relevant dimensionless space variables reflecting the difference of characteristic sizes along axial and transverse directions are $(x_1/L,\ x_2/l,\ x_3/l)$. Equivalently, the appropriate physical space variables are $(x_1,\ y_2,\ y_3)$, where $y_\alpha = (L/l)x_\alpha = \epsilon_b^{-1}x_\alpha$ (by convention, the greek indices take values 2 and 3, e.g. $\underline{y} = y_\alpha \underline{a}_\alpha$). Now, for a quantity φ expressed in function of $(x_1, \underline{y})$ the usual gradient operator $\nabla\varphi(\underline{x}) = (\partial_{x_i}\underline{a}_i)\varphi(\underline{x})$ becomes $\nabla\varphi(x_1, \underline{y}) = (\partial_{x_1}\underline{a}_1 + \epsilon_b^{-1}\partial_{y_\alpha}\underline{a}_\alpha)\varphi(x_1, \underline{y})$, and similarly for the divergence and other differential operators. It results that the balance equations involves terms of different orders of magnitude in ϵ_b.

Second, the specificity of the axial direction leads to decompose the symmetric tensor of strain ($\underline{\underline{e}}^{\mathcal{B}}$) or stress ($\underline{\underline{\sigma}}^{\mathcal{B}}$) into reduced tensors, e.g. for the stress:

$$\underline{\underline{\sigma}}^{\mathcal{B}} = \sigma_{\mathrm{N}}\underline{a}_1 \otimes \underline{a}_1 + (\underline{\sigma}_{\mathrm{T}} \otimes \underline{a}_1 + \underline{a}_1 \otimes \underline{\sigma}_{\mathrm{t}}) + \underline{\underline{\sigma}}_{\mathrm{S}}$$

where, the three reduced tensors are:

$\sigma_{\mathrm{N}} = \sigma_{11}$: the *scalar* axial stress,

$\underline{\sigma}_{\mathrm{T}} = \sigma_{1\alpha}\underline{a}_\alpha$: the 2D stress *vector* exerted *out of the plane* of the section,

$\underline{\underline{\sigma}}_{\mathrm{S}} = \sigma_{\alpha\beta}(\underline{a}_\alpha \otimes \underline{a}_\beta + \underline{a}_\beta \otimes \underline{a}_\alpha)/2$: the 2D stress *tensor in the plane* of the section.

Third, the existence of terms of different orders of magnitude in the balance equation leads to seek for the variables in the form of asymptotic expansion in power of ϵ_b, e. g. $\varphi(x_1, \underline{y}) = \varphi^{(0)}(x_1, \underline{y}) + \epsilon_b\varphi^{(1)}(x_1, \underline{y}) + \epsilon_b^2\varphi^{(2)}(x_1, \underline{y}) + \ldots$. The process consists in introducing the expansions in the balance equations. Separating the terms of different orders leads to a series of problems to be solved successively (refer to Appendix A for further details). Following this procedure, the classic Euler-Bernoulli kinematics under flexural motions along $\underline{a}_3$ is recovered at the leading order, that is

$$\underline{u}^{(0)}(x_1, \underline{y}) = U(x_1)\underline{a}_3 \qquad ; \quad \underline{u}^{(1)}(x_1, \underline{y}) = -y_3\partial_{x1}U\underline{a}_1$$

As for the three reduced stress tensors, it comes out that their orders of magnitude differ, namely:

$$\sigma_N = \epsilon_b O\left(E_b\frac{U}{L}\right); \qquad \underline{\sigma}_T = \epsilon_b^2 O\left(E_b\frac{U}{L}\right); \qquad \underline{\underline{\sigma}}_S = \epsilon_b^3 O\left(E_b\frac{U}{L}\right)$$

Furthermore, it shown that σ_N and $\underline{\underline{\sigma}}_S$ expand in odd powers of ϵ_b, while $\underline{\sigma}_T$ expands in even powers of ϵ_b. In other words, at the leading order, the stress tensor in the beam $\underline{\underline{\sigma}}^{\mathcal{B}}$ reads:

$$\begin{aligned}\underline{\underline{\sigma}}^{\mathcal{B}} &= \epsilon_b\sigma_N^{(1)}\underline{a}_1 \otimes \underline{a}_1 + \epsilon_b^2\sigma_{T1\alpha}^{(2)}(\underline{a}_1 \otimes \underline{a}_\alpha + \underline{a}_\alpha \otimes \underline{a}_1) \\ &\quad + \epsilon_b^3\sigma_{S\alpha\beta}^{(3)}(\underline{a}_\alpha \otimes \underline{a}_\beta + \underline{a}_\beta \otimes \underline{a}_\alpha)\end{aligned} \tag{6}$$

so that the stress vector on the surface Γ_b in contact with the plate takes the form

$$\underline{\underline{\sigma}}^{\mathcal{B}}.\underline{a}_2 = \epsilon_b^2\sigma_{T12}^{(2)}\underline{a}_1 + \epsilon_b^3(\sigma_{S22}^{(3)}.\underline{a}_2 + \sigma_{S23}^{(3)}.\underline{a}_3)$$

Finally the $\underline{a}_3$-transverse vibrations of the beam element $\mathcal{B}$, are described by the following equations expressing respectively, the transverse force balance along $\underline{a}_3$ axis, the balance of couple according to $\underline{a}_2$, and the bending constitutive law:

$$\begin{cases} \partial_{x_1}T^{\mathcal{B}} + \left(\displaystyle\int_{\Gamma_b^+}\sigma_{S23} - \int_{\Gamma_b^-}\sigma_{S23}\right) = -\Lambda_b\omega^2 U(x_1) \\ \partial_{x_1}M^{\mathcal{B}} + \left(\displaystyle\int_{\Gamma_b^+} y_3\sigma_{T12} - \int_{\Gamma_b^-} y_3\sigma_{T12}\right) - T_3^{\mathcal{B}} = 0 \\ M^{\mathcal{B}} = -E_bI_b\partial_{x_1}^2 U(x_1) \end{cases} \tag{7}$$

The coupling with the plate arises from the terms in parenthesis in (7). It consists in (i) a shear force associated with the stresses $\sigma_{S23} = \epsilon_b^3\sigma_{S23}^{(3)}$ and in (ii) a $\underline{a}_2$-couple related to $\sigma_{T12} = \epsilon_b^2\ \sigma_{T12}^{(2)}$. The stress $\sigma_{S22} = \epsilon_b^3\sigma_{S22}^{(3)}$ normal to Γ_b has no effect since at the leading order the beam section undergoes a rigid body motion with zero in-plane deformation. In particular Γ_b^- and Γ_b^+ follows the same motion $U(x_1)$.

3.1.2. Asymptotic model for the plate $\mathcal{P}$

The plate satisfies the flatness criterion $\epsilon_p = d/D \ll 1$. The plate geometry naturally differentiates the in-plane $(\underline{a}_1,\ \underline{a}_2)$ and out-of-plane $\underline{a}_3$ directions ; and the in-plane variations occurs according to D while the variation across the plate thickness arise according to d. Consequently, the appropriate physical space variables describing the plate are $(x_1,\ x_2,\ y_3)$, where $y_3 = (D/d)x_3 = \epsilon_p^{-1}x_3$, so that the usual gradient operator $\nabla\varphi(\underline{x}) = (\partial_{x_i}\underline{a}_i)\varphi(\underline{x})$ becomes $\nabla\varphi(x_1, x_2, y_3) = (\partial_{x_1}\underline{a}_1 + \partial_{x_2}\underline{a}_2 + \epsilon_p^{-1}\partial_{y_3}\underline{a}_3)\varphi(x_1, x_2, y_3)$. The terms of different order of magnitude in the balance equation lead to seek for the variables in the form of asymptotic expansions in power of ϵ_p, e.g. $\varphi(x_1, x_2, y_3) = \varphi^{(0)}(x_1, x_2, y_3) + \epsilon_p\varphi^{(1)}(x_1, x_2, y_3) + \epsilon_p^2\varphi^{(2)}(x_1, x_2, y_3) + \ldots$.

Now, in accordance with the flat geometry, the stress tensor ($\underline{\underline{\sigma}}^{\mathcal{P}}$) is decomposed into (the same decomposition applies to the strain tensor):

$$\underline{\underline{\sigma}}^{\mathcal{P}} = \underline{\underline{\sigma}}_{\mathrm{p}} + (\underline{\sigma}_{\mathrm{t}} \otimes \underline{a}_3 + \underline{a}_3 \otimes \underline{\sigma}_{\mathrm{t}}) + \sigma_{\mathrm{n}}\underline{a}_3 \otimes \underline{a}_3$$

where, the reduced tensors of the plate reads (with indices $a, b = \{1, 2\}$):

$\underline{\underline{\sigma}}_{\mathrm{p}} = \sigma_{ab}(\underline{a}_a \otimes \underline{a}_b + \underline{a}_b \otimes \underline{a}_a)$: the 2D second rank *tensor* of the strain or stress *in the plane* of the plate,

$\underline{\sigma}_{\mathrm{t}} = \sigma_{3a}\underline{a}_a$: the 2D strain or stress *vector* exerted *out of the plane* of the plate,

$\sigma_{\mathrm{n}} = \sigma_{33}$: the *scalar* out-of-plane normal stress or strain.

The asymptotic resolution is close to that for the beam, the main difference lying in the fact that the spatial variable associated with the $\underline{a}_2$ axis is microscopic in the beam but macroscopic for the plate. The resolution at the leading order leads to a Love–Kirchhoff plate where the dominating kinematic variable $w(x_1, x_2) < uline > a < /uline >_3$ is the out-of-plane displacement of $\mathcal{P}$. The reduced stress tensors, are of different orders of magnitude given by:

$$\underline{\underline{\sigma}}_p = \epsilon_p O\left(E'_p\frac{w}{D}\right) \quad ; \quad \underline{\sigma}_t = \epsilon_p^2 O\left(E'_p\frac{w}{D}\right) \quad ; \quad \sigma_n = \epsilon_p^3 O\left(E'_p\frac{w}{D}\right)$$

and, it is shown that their expansion is in odd (respectively even) ϵ_p powers for $\underline{\underline{\sigma}}_p$ and σ_n (respectively $\underline{\sigma}_t$). Hence, at the leading order, the stress tensor in the plate $\underline{\underline{\sigma}}^{\mathcal{P}}$ reads:

$$\begin{aligned}\underline{\underline{\sigma}}^{\mathcal{P}} &= \epsilon_p\underline{\underline{\sigma}}_{pab}^{(1)}(\underline{a}_a \otimes \underline{a}_b + \underline{a}_b \otimes \underline{a}_a) \\ &\quad + \epsilon_p^2\sigma_{t3a}^{(2)}(\underline{a}_3 \otimes \underline{a}_1 + \underline{a}_1 \otimes \underline{a}_3) + \epsilon_p^3\sigma_n^{(3)}\underline{a}_3 \otimes \underline{a}_3\end{aligned} \tag{8}$$

As a result, the stress vector at the junction Γ_p with the beam is given by:

$$\underline{\underline{\sigma}}^{\mathcal{P}}.\underline{a}_2 = \epsilon_p(\sigma_{p12}^{(2)}\underline{a}_1 + \sigma_{p22}^{(2)}\underline{a}_2) + \epsilon_p^2\sigma_{t32}^{(3)}.\underline{a}_3$$

It results that, at the leading order, the out-of-plane $\underline{a}_3$-vibrations of the plate element $\mathcal{P}$ are described by the set of Eq. (9) expressing respectively, the in-plane balance of transverse force balance along $\underline{a}_3$ axis, the in-plane balance of the tensor of the in-plane oriented couples, and the bending constitutive law:

$$\begin{cases} \widetilde{\mathrm{div}}(\underline{T}^{\mathcal{P}}) = -\Lambda_p \omega^2 w \\ \widetilde{\underline{\mathrm{div}}}(\underline{\underline{M}}^{\mathcal{P}}) - \underline{T}^{\mathcal{P}} = 0 \\ \underline{\underline{M}}^{\mathcal{P}} = -E'_p I_p((1-\nu_p)\widetilde{\underline{\underline{e}}}(\widetilde{\underline{\nabla}} w) + \nu_p \widetilde{\Delta} w \underline{\underline{I}}_p) \end{cases} \tag{9}$$

In the above equations the 'tilded' differential operator stand for the in-plane operator. For instance $\widetilde{\underline{\nabla}} = \partial_{x_1}\underline{a_1} + \partial_{x_2}\underline{a_2}$; $\widetilde{\underline{\underline{e}}}(\underline{u}) = (\widetilde{\nabla}(\underline{u}) +^t \widetilde{\nabla}(\underline{u}))/2$; $\widetilde{\mathrm{div}}(\underline{T}) = \partial_{x_1} T_1 + \partial_{x_2} T_2$; etc.

3.2. Homogenized bending model of ribbed plate

The above elements enable to determine the model of periodic ribbed plates assuming that the wavelength carried by the beams of characteristic size L (the forcing constituent) is much larger than the size D of the period Ω, consistently with the fact that $D/L = \varepsilon \ll 1$.

It follows that the gradient of the displacement along x_1 and x_2 differs significantly, namely $\partial_{x_1} U = O(U/L) \ll \partial_{x_2} w = O(w/D)$ so that, since $w = O(U)$:

$$\partial_{x_1} w = O(\varepsilon \partial_{x_2} w) \ll \partial_{x_2} w \tag{10}$$

Furthermore, as a consequence of the scale separation and of the Ω-periodicity, the physical variables take identical values on both sides of Ω, i.e. on Γ_b^- and Γ_p^+.

By construction, the beam and plate models (7), (9) already express the dynamic equilibrium within both constituents $\mathcal{B}$ and $\mathcal{P}$. Consequently, to fulfill the dynamic balance of the whole cell Ω, it remains to formulate the balance at the junction Γ which will specify the beam/plate coupling. In this aim, the dynamic field within plate $\mathcal{P}$ has to be determined explicitly.

3.2.1. Dynamic regime of the plate driven by the beam motion

Let us specify the leading order boundary conditions on plate extremities Γ_p. The beam and plate displacements are identical at their interfaces, i.e., $w_{\Gamma_p^-} = U_{\Gamma_b^+}$, and, by periodicity, $w_{\Gamma_p^+} = U_{\Gamma_b^-}$. In addition, since the beam section undergoes a rigid body motion at the leading order, consequently *i)* $U_{\Gamma_b^-} = U_{\Gamma_b^+}$, this implies a Dirichlet boundary condition on Γ_p that is $W(x_1, x_{2|\Gamma_p}) = U(x_1)$, where $W(x_1, x_2)$ stands for the leading order term of the expansion of w, i.e. $W(x_1, x_2) = w^{(0)}(x_1, x_2)$, and *ii)* the motion of the plate connected at the interface Γ_p is normal to $\underline{a}_2$. This implies that a clamped condition applies on the plate extremities, i.e. $\partial_{x_2} W(x_1, x_{2|\Gamma_p}) = 0$.

Now, condition (10) $\partial_{x_1} W \ll \partial_{x_2} W$ states that the 2D plate Eq. (9) reduces to a 1D equation involving x_2 only. To sum up, the elasto-dynamic equations describing the plate $\mathcal{P}$ in conditions of scale separation and periodicity read:

$$\text{in } \mathcal{P} \quad \begin{cases} \partial_{x_2} T^{\mathcal{P}} = -\Lambda_p \omega^2 W \\ \partial_{x_2} M^{\mathcal{P}} - T^{\mathcal{P}} = 0 \\ M^{\mathcal{P}} = -E'_p I_p \partial^2_{x_2} W \end{cases} \qquad \text{on } \Gamma_p \quad \begin{cases} \forall x_1 \\ W(x_1, x_{2|\Gamma}) = U(x_1) \\ \partial_{x_2} W(x_1, x_{2|\Gamma}) = 0 \end{cases} \tag{11}$$

It results that, (i) x_1 plays the role of a parameter involved on the boundary condition only and, (ii) the set (11) is a linear problem where the displacement $U(x_1)$ is the forcing term. Thus, $W(x_1, x_2)$ takes the form

$$W(x_1, x_2) = U(x_1)\phi_\omega(x_2) \tag{12}$$

where $\phi_\omega(x_2)$ is the frequency dependent solution of the one-dimensional harmonic bending equation here below in which appears the natural flexural wavenumber δ defined by (as well as the dimensionless wave number δ^*)

$$\delta^4 = \Lambda_p \omega^2 / (E'_p I_p) \quad ; \quad \delta^* = \delta D/2$$

$$\partial^4_{x_2}\phi_\omega - \delta^4 \phi_\omega = 0\,; \quad \phi_\omega(x_{2|\Gamma}) = 1\,; \quad \partial_{x_2}\phi_\omega(x_{2|\Gamma}) = 0 \tag{13}$$

The resolution of (13) is straightforward and the solution reads

$$\phi_\omega(x_2) = \frac{\cosh(\delta x_2)\sin(\delta^*) + \cos(\delta x_2)\sinh(\delta^*)}{\cosh(\delta^*)\sin(\delta^*) + \cos(\delta^*)\sinh(\delta^*)} \quad ; \quad -D/2 < x_2 < D/2 \tag{14}$$

The expression of $\phi_\omega(x_2)$ highlights the resonant character of the plate response. The vanishing of the denominator leads to an infinite motion. This occurs at the specific series of frequencies corresponding to the odd modes, that are symmetric, of the plate (see the Remark below). Note that, in accordance with the symmetry of the forced boundary conditions, the antisymmetric modes of the clamped plate do not participate to the forced motion ϕ_ω. It is useful for the following to introduce $\langle\phi_\omega\rangle$ the mean value of ϕ_ω

$$\langle\phi_\omega\rangle = \frac{1}{D}\int_{-D/2}^{D/2} \phi_\omega(x_2)\mathrm{d}x_2 = \frac{2}{\delta^*}\frac{1}{\coth(\delta^*) + \cot(\delta^*)} \tag{15}$$

Remark: The eigenfrequencies $\{\omega_I\}$ associated to the eigenmodes $\{\Psi^I\}$ of a clamped plate in one-dimensional bending are given by series of roots $\{\delta_I^*\}$, $\{I = 1, 2, 3, \dots\}$ of the transcendental equation

$$F(\delta^*) = 0 \quad \text{where} \quad F(\delta^*) = \cosh(2\delta^*)\cos(2\delta^*) - 1$$

As this equation can be also expressed as

$$f_+(\delta^*) f_-(\delta^*) = 0 \quad \text{where} \quad f_\pm(\delta^*) = \tan(\delta^*) \pm \tanh(\delta^*)$$

the roots $\{\delta_I^*\}$ are split into (i) the subset $\{\delta^*_{2n+1}\}$ roots of $f_+(\delta^*) = 0$ associated to the n^{th} odd $(I = 2n-1)$ and symmetric modes $\Psi^n_s = \Psi^{2n-1}$, and (ii) the subset $\{\delta^*_{2n}\}$ roots of $f_-(\delta^*) = 0$ associated to the n^{th} even $(I = 2n)$ and antisymmetric modes $\Psi^n_t = \Psi^{2n}$. For $I > 1$ the $\{\delta_I^*\}$ are closely approximated by $\{\delta_I^*\} \approx \frac{\pi}{2}(I + \frac{1}{2})$.

Thus the eigenfrequencies $\{\omega_{sn}\}$ of the symmetric modes take values close to

$$\omega_{sn} \approx (2n - \frac{1}{2})^2 \left(\frac{\pi}{D}\right)^2 \sqrt{\frac{E_p I_p}{\Lambda_p}} \qquad , \qquad n = (1), 2, 3, \dots$$

while the eigenfrequencies $\{\omega_{tn}\}$ of the anti symmetric modes take values close to

$$\omega_{tn} \approx (2n + \frac{1}{2})^2 \left(\frac{\pi}{D}\right)^2 \sqrt{\frac{E_p I_p}{\Lambda_p}} \qquad , \qquad n = 1, 2, 3, \dots$$

3.2.2. Beam/plate coupling

We are now in position to determine the coupling terms in the beam balance (7). From the displacement field in the plate one deduces the stress state and then the force and couple at the plate extremities. The in-plane stress σ_{p12} reads

$$\sigma_{p12} = -E'_p(1-\nu_p) y_3 \partial^2_{x_1 x_2} W$$

and due to the clamped condition $\partial_{x_2} W = 0$ on Γ_p, both the shear stress and the $\underline{a}_2$-couple are null at the plate extremities Γ_p^+ and Γ_p^-, i.e. $\sigma_{p12|\Gamma_p^\pm} = 0$ thus $\int_{\Gamma_p^\pm} y_3 \sigma_{p12} = 0$. As for the transverse shear force on the plate extremities we have

$$T^{\mathcal{P}}_{|\Gamma_p^\pm} = \int_{\Gamma_p^\pm} \sigma_{t23} = E'_p I_p (\partial^3_{x_2} W)_{|\Gamma_p^\pm} = E'_p I_p U(x_1)(\partial^3_{x_2}\phi_\omega)_{|\Gamma_p^\pm}$$

Expressing the beam/plate stress continuity $\underline{\underline{\sigma}}^{\mathcal{B}}.\underline{a}_2 = \underline{\underline{\sigma}}^{\mathcal{P}}.\underline{a}_2$ at their interface (i.e. the interface balance) and accounting for the periodicity we have:

$$\sigma_{T12|\Gamma_b^\mp} = \sigma_{p12|\Gamma_p^\pm} = 0 \quad ; \quad \sigma_{S23|\Gamma_b^\mp} = \sigma_{t23|\Gamma_p^\pm}$$

Then the couple and force exerted by the plate on the beam (see (7)) read

$$\int_{\Gamma_b^+} y_3\sigma_{T12} - \int_{\Gamma_b^-} y_3\sigma_{T12} = \int_{\Gamma_p^-} y_3\sigma_{p12} - \int_{\Gamma_p^+} y_3\sigma_{p12} = 0 \tag{16}$$

$$\int_{\Gamma_b^+} \sigma_{S23} - \int_{\Gamma_b^-} \sigma_{S23} = \int_{\Gamma_p^-} \sigma_{t23} - \int_{\Gamma_p^+} \sigma_{t23} = T^{\mathcal{P}}_{|\Gamma_p^-} - T^{\mathcal{P}}_{|\Gamma_p^+}$$

It is worth noticing that the matching of the integrated values of the non vanishing stresses $\int_{\Gamma_b} \sigma_{S23} = \int_{\Gamma_b^-} \epsilon_b^3\sigma^{(3)}_{S23}$ and $\int_{\Gamma_p^+} \sigma_{t23} = \int_{\Gamma_p} \epsilon_p^2\sigma^{(2)}_{t32}$ requires that both terms are of the same order. This is actually provided when the scaling (3) is satisfied. Indeed, as the reference values that normalize the stresses are $E_b\frac{U}{L}$ and $E_p\frac{U}{D}$ in the beam and plate respectively, then $\int_{\Gamma_b} \epsilon_b^3\sigma^{(3)}_{S23} = O(l.(\frac{l}{L})^3 E_b\frac{U}{L}$ and $\int_{\Gamma_p} \epsilon_p^2\sigma^{(2)}_{t32} = O(d.(\frac{d}{D})^2 E_p\frac{U}{D})$, so that equating the order of both terms leads to (3).

Furthermore, from the plate Eq. (11)

$$\begin{aligned} T^{\mathcal{P}}_{|\Gamma_p^-} - T^{\mathcal{P}}_{|\Gamma_p^+} &= -\int_{-D/2}^{D/2} \partial_{x_2} T^{\mathcal{P}} \mathrm{d}x_2 = \Lambda_p\omega^2 \int_{-D/2}^{D/2} W \mathrm{d}x_2 \\ &= \Lambda_p D\langle\phi_\omega\rangle\omega^2 U(x_1) \end{aligned} \tag{17}$$

Relations (16) and (17) show that the plate does not induce any $\underline{a}_2$-couple on the beam, but exerts a shear force on the form of a inertial term with a non-conventional frequency dependence arising from $\langle\phi_\omega\rangle$. This expression reported in (7) provides the effective modeling of the ribbed plates, that involves the beam deflection $U(x_1)$ as the unique kinematic descriptor.

3.2.3. Dynamic regime of the plate with passive beams

Implicitly, the above analysis assumes that the beams are moving and, in turn, determine the dynamics of the whole ribbed plate. However, such a regime disappears when the beam are passive, i.e., when $U(x_1) = u^{(0)} = 0$ (meaning that the beam displacement expansion begin at the first order i.e. $u = \epsilon_b u^{(1)} + \dots$) so that the forcing of the plate vanishes at the leading order. Nonetheless, an other mechanism of vibration with passive beams is possible. The latter is defined in each plate $\mathcal{P}$ by (9) together with the fixed and clamped conditions on Γ_p at the leading order. The plate motion $W(x_1, x_2) = w^{(0)}(x_1, x_2)$ is the unique kinematic descriptor of this dynamic regime. Note that, to insure a null beam deflection, the shear forces exerted by the plates on the opposite sides of the beam section must vanish. This imposes that in two adjacent plates the motions are identical but of opposite sign. Hence, the kinematic of the whole ribbed plate with passive beams is fully determined.

3.2.4. Synthetic formulation of the flexural behavior of ribbed plates

The above analysis of the flexural motions of the ribbed plate leads to a dual formulation that encompasses the two independent types of flexural behaviors. The first one is associated with moving beams which make the plate vibrating, while in the second one the plates only are set in vibration.

- the case where the beam is active $U(x_1) \neq 0$ gives the global modes associated with the flexural inertia of the beam and a non conventional effective beam/plate inertia that includes the static mass of the beam and the frequency-dependent effective mass of the plate. This situation actually describes a co-dynamic beam/plate regime and the corresponding equation for the beam deflection $U(x_1)$ reads:

$$\begin{aligned} &E_b I_b \partial^4_{x_1} U = \omega^2(\Lambda_b + \Lambda_p D\langle\phi_\omega\rangle)U; \\ &\langle\phi_\omega\rangle = \frac{2}{\delta^*}\frac{1}{\coth(\delta^*) + \cot(\delta^*)} \end{aligned} \tag{18}$$

- the case where the beam is passive $U(x_1) = 0$ leads to guided modes governed by the flexural inertia and the surface mass of the plate. The corresponding equation for the plate deflection $W(x_1, x_2)$ reads:

$$\begin{aligned} E'_p I_p \widetilde{\Delta}^2 W = \Lambda_p\omega^2 W \quad &\text{with on } \Gamma_p \quad W(x_1, x_{2|\Gamma_p}) = 0 \quad ; \\ &\partial_{x_2} W(x_1, x_{2|\Gamma_p}) = 0 \end{aligned} \tag{19}$$

and, as above explained, one has alternatively W and $-W$ from a plate to the adjacent one.

4. Dispersion features of ribbed plates in bending

4.1. Bending waves with active beams

Let us first outline the strong frequency dependence of the apparent dimensionless mass $\langle\phi_\omega\rangle$ of $\mathcal{P}$. According to (15) and recalling that $\omega = \delta^2\sqrt{\frac{E'_p I_p}{\Lambda_p}}$ and $\delta^* = \delta D/2$ we have:

- $\langle\phi_\omega\rangle \to 1$ when $\delta^* \to 0$ i.e. when $\omega \to 0$, which is consistent with the fact that in statics, the apparent mass of $\mathcal{P}$ is the real mass,
- $\langle\phi_\omega\rangle \to \pm\infty$ when $\tan(\delta^*) + \tanh(\delta^*) = 0$ which corresponds to the eigenfrequencies $\{\omega_{sn}\}$ of the symmetric $\mathcal{P}$-plate modes. When $\omega \to \omega_{sn}^-$, the plate apparent mass tends to be infinite and positive, while it tends to negative infinite values when $\omega \to \omega_{sn}^+$,
- $\langle\phi_\omega\rangle = 0$ when $\delta^* = \pi(n + 1/2)$, i.e. at frequencies $\omega_{0n} = (2n+1)^2\left(\frac{\pi}{D}\right)^2\sqrt{\frac{E_p I_p}{\Lambda_p}}$ that lies in-between ω_{sn} and $\omega_{s(n+1)}$. Thus in the intervals $[\omega_{sn}, \omega_{0n}]$ the apparent mass of $\mathcal{P}$ is negative.

In practice, the singularities of $\langle\phi_\omega\rangle$ are smoothed by the unavoidable dissipation effects. They can be accounted for through a structural damping η introduced as a corrective imaginary part of the elastic modulus that becomes $(1 + i\eta)E_p$. Quantities are then complex-valued and smoothing appears as η is increased.

The properties of $\langle\phi_\omega\rangle$ are illustrated in Fig. 2 that presents for two values of damping the variations of the real and imaginary parts versus the frequency normalized by the fundamental frequency. Except in the neighborhood of the eigenmodes where $\langle\phi_\omega\rangle$ becomes singular, $\langle\phi_\omega\rangle$ is globally confined between 1 and 0 and the modal mass diminishes as ω increases. This means that, for intermediate frequencies in between the eigenfrequencies, the plate behaves as if it were lighter than it actually is.

Considering a wave propagating along x_1 of the form $U(x_1) = \exp(ik_\omega x_1)$, the dispersion features of waves governed by (19) is determined by the flexural wavenumber k_ω given by

$$k_\omega^4 = \omega^2\frac{\Lambda_b + \Lambda_p D\langle\phi_\omega\rangle}{E_b I_b} \tag{20}$$

Due to the inner resonance of plate $\mathcal{P}$ accounted by $\langle\phi_\omega\rangle$, the dispersion Eq. (20) differs notably from the classical bending case in which $k \sim \sqrt{\omega}$ in the whole frequency range, especially in the neighborhood of the eigenmodes. In particular, slow down bending waves (compared to that in beam $\mathcal{B}$) appear around ω_{sn}^-, where $\langle\phi_\omega\rangle \gg 1$. Furthermore, within the range $[\omega_{sn}, \omega_{0n}]$ in which $\langle\phi_\omega\rangle < 0$ and/or $|\langle\phi_\omega\rangle| \gg 1$, either strongly damped bending waves (similarly to thermal waves) occur if $k^4 < 0$ so that $k \sim \sqrt{i}$, or bending waves can be speed up if $k^4 \approx 0$ and is positive. The numerical evidences of these properties are detailed in Section 6.

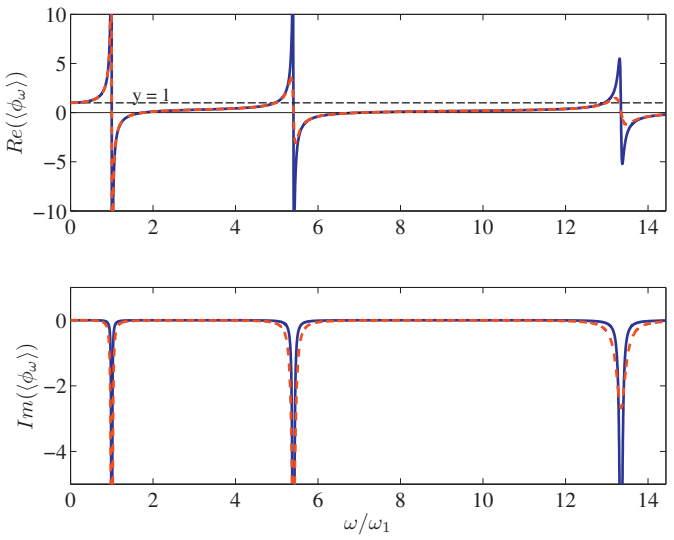

Fig. 2. Real and imaginary parts of the dimensionless apparent mass of the plate $\langle\phi_\omega\rangle$ versus dimensionless circular frequency ω/ω_{s1} of the three first symmetric modes; with structural damping $\eta = 0.5\%$ (—) , and $\eta = 2\%$ (– –).

4.2. Bending waves with passive beams

Focusing on the second mechanism when the beams are at rest (19), the plate is clamped on its two opposite sides, however a long wavelength motion is possible along its length L. The exact determination of the dispersion of these guided waves would require a numerical resolution. However, the dispersion features can be fairly assessed by approximating the field within the plate. We present here two simple options for assessing the dispersion relation of these guided waves.

Let us seek for an approximated solution in the form of separated variables:

$$w(x_1,x_2) = \exp(ik'_\omega x_1)\Psi(x_2) \qquad \text{where}$$
$$\Psi(x_{2|\Gamma_p}) = 0 \quad ; \quad \partial_{x_2}\Psi(x_{2|\Gamma_p}) = 0$$

The function $\Psi(x_2)$ fluctuates according to the plate width D, while $\exp(ik'_\omega x_1)$ varies according to $L \gg D$. Consequently, at the leading order, the plate equation reduces to the following 1D-problem (identical to (11) except for the zero boundary condition for Ψ):

$$E'_p I_p \partial^4_{x_2}\Psi = \Lambda_p\omega^2\Psi \qquad \Psi(x_{2|\Gamma_p}) = 0 \quad ; \quad \partial_{x_2}\Psi(x_{2|\Gamma_p}) = 0$$

The solutions are the modes (symmetric and non symmetric) $\Psi^I(x_2)$ associated with the infinite series of frequencies ω_I. Hence, $w(x_1, x_2)$ appears to be the x_2-eigenmodes modulated according to large wavelength along x_1. The x_1-wave number can then be determined by reporting the expression of $w(x_1, x_2)$, in the bilaplacian Eq. (19) governing the plate $\mathcal{P}$. For each eigenmode Ψ^I one obtains:

$$E'_p I_p\Big[(k'^I_\omega)^4\Psi^I - 2(k'^I_\omega)^2\partial^2_{x_2}\Psi^I + \partial^4_{x_2}\Psi^I\Big] = \Lambda_p\omega^2\Psi^I$$

that is, since, $E'_p I_p\partial^4_{x_2}\Psi^I = \Lambda_p\omega_I^2\Psi^I$:

$$E'_p I_p\Big[(k'^I_\omega)^4\Psi^I - 2(k'^I_\omega)^2\partial^2_{x_2}\Psi^I\Big] = \Lambda_p(\omega^2 - \omega_I^2)\Psi^I \tag{21}$$

- At this step, a first approach consists in integrating this equation over to x_2. Noticing that $\int\partial^2_{x_2}\Psi^I = [\partial_{x_2}\Psi(x_2)]_{|\Gamma_p} = 0$, one derives

$$E'_p I_p(k'^I_\omega)^4\langle\Psi^I\rangle = \Lambda_p(\omega^2 - \omega_I^2)\langle\Psi^I\rangle$$

This leads to an approximated dispersion equation associated with the mode Ψ^I that simply reads

$$(k'^I_\omega)^4 \approx \frac{\Lambda_p}{E'_p I_p}(\omega^2 - \omega_I^2) \tag{22}$$

- An alternative approach is to approximate the exact eigenmode shapes of the clamped plate that are given by ($0 \le x_2 \le D$ and $\delta^*_I = \delta(\omega_I)D/2$):

$$\Psi^I(x_2) = \cos\left(\delta^*_I(\frac{2x_2}{D} - 1)\right) + \frac{\sin(\delta^*_I)}{\sinh(\delta^*_I)}\cosh\left(\delta^*_I(\frac{2x_2}{D} - 1)\right); \qquad (I = 2n = 2, 4, 6, \ldots)$$

$$\Psi^I(x_2) = \sin\left(\delta^*_I(\frac{2x_2}{D} - 1)\right) - \frac{\sin(\delta^*_I)}{\sinh(\delta^*_I)}\sinh\left(\delta^*_I(\frac{2x_2}{D} - 1)\right); \qquad (I = 2n+1 = 1, 3, 5, \ldots)$$

where the values of δ^*_I are the roots of $\tan(\delta^*_I) + (-1)^I\tanh(\delta^*_I) = 0$.
Since the roots δ^*_I are very close to the series $\frac{\pi}{2}(I + \frac{1}{2})$ the mode shape functions can be approximated by $\Psi^I(x_2) \approx \sin(I\pi\frac{x_2}{D})$ so that $\partial^2_{x_2}\Psi^I \approx -(\frac{I\pi}{D})^2\Psi^I$ (note that these expressions are compatible with the sign inversion of the motions from a plate the adjacent one). Reporting this approximation in (21) yields the following approximated dispersion equation for the guided waves

$$(k'^I_\omega)^4 + 2(k'^I_\omega)^2\left(\frac{I\pi}{D}\right)^2 - \frac{\Lambda_p}{E'_p I_p}(\omega^2 - \omega_I^2) \approx 0 \tag{23}$$

We will see in Section 6 that (23) provides better estimates than (22). The family (indexed by the eigenmode number I) of equations (23) defines the guided waves branches. The features of these waves are defined by the nature of the roots of (23) that depends strongly upon the frequency. Simple algebra shows that the discriminant is negative for $\omega < \omega_{cI}$ and positive above, ω_{cI} being given by

$$\omega^2_{cI} = \omega_I^2\left(1 - \frac{I^4}{(I + \frac{1}{2})^4}\right) < \omega_I^2$$

Hence, at frequencies lower than ω_{cI}, the wavenumbers are complex valued which corresponds to propagative but significantly damped waves. For frequencies in the interval $[\omega_{cI},\ \omega_I]$ the wavenumbers are imaginary, so that the waves are evanescent in this range. Finally for frequencies higher than the clamped plate eigenfrequencies ω_I, a real positive root exists and the wave propagates without damping. Note also that these guided waves are build in a similar manner for the symmetric or the non symmetric modes of the clamped plate. Their features will be illustrated in Section 6.

4.3. Limit of validity the homogenized model

It is worth recalling the conditions of validity of the homogenized model. As for the beam and plate models itself, the frequency must be sufficiently low to fulfill the slenderness and flatness requirement in dynamic regime. This imposes the classical following restrictions on the reduced wavelengths $\mathcal{L}_{\mathcal{B}_\omega} > l$ and $\mathcal{L}_{\mathcal{P}_\omega} > d$ that read:

$$\omega^2 < \text{Min}\left\{\frac{E_b I_b}{\Lambda_b l^4},\ \frac{E'_p I_p}{\Lambda_p d^4}\right\} \tag{24}$$

In addition, for the ribbed plate, the scale separation must be satisfied, i.e., $k_\omega D < 1$, that corresponds to the frequencies ranges such

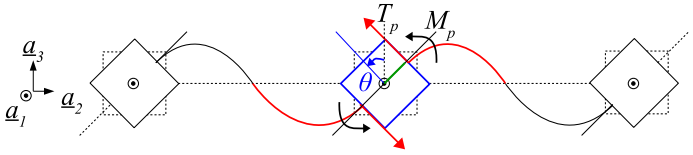

Fig. 3. Torsional kinematics with torque applied by the plate and moment induced in the beam.

that

$$\omega^2 < \frac{E_b I_b}{(\Lambda_b + \Lambda_p D\langle\phi_\omega\rangle)D^4} \tag{25}$$

The modeling (18) with active beams only applies if both conditions (24) and (25) are fulfilled. However, modeling (19) with passive beams and guided waves in the plates applies if the single condition $\omega^2 < \frac{E'_p I_p}{\Lambda_p d^4}$ is satisfied.

5. Homogenized formulation of the torsional behavior of ribbed plates

The analysis of the bending behavior can be replicated for studying the dynamic torsional behavior. Fig. 3 depicts the torsional kinematics of the ribbed plate : the beam $\mathcal{B}$ in torsion imposes its rotation to the plate extremities, in turn the plate $\mathcal{P}$ is bended and exerts shear forces and torques on the beam. The requirements for reaching this situation are identified by expressing the conditions of "co-dynamic" regime and of asymmetric coupling.

The equation describing the dynamic torsion of the beam $\mathcal{B}$ alone (i.e. not connected to the plate) along its axis $\underline{a}_1$ reads (see axis of Fig. 3)

$$G_b\mathcal{I}_b\partial^2_{x_1}\theta = -\rho_b J_b\omega^2\theta$$

where θ is the torsion angle, $G_b\mathcal{I}_b$ the torsional rigidity of the beam and $\rho_b J_b$ its polar moment, with $G_b = E_b/2(1+\nu_b)$, $\mathcal{I}_b = O(l^4)$, $J_b = O(l^4)$. Thus, the reduced wavelength in torsion $\mathcal{L}'_\omega$ reads:

$$\mathcal{L}'^2_\omega = O\left(\frac{G_b\mathcal{I}_b}{\rho_b J_b\omega^2}\right)$$

At the fundamental resonance in torsion ω'_b of the beam of length L', $\mathcal{L}'_\omega = L'$ so that:

$$\omega'^2_b = O\left(\frac{G_b\mathcal{I}_b}{\rho_b J_b L'^2}\right)$$

Concerning the plate $\mathcal{P}$, its resonance frequency in bending is of the order of : $\omega_p^2 = O\left(\frac{E'_p I_p}{\Lambda_p D^4}\right)$. Then, considering again the inner resonance situation where the fundamental frequencies of the beam $\mathcal{B}$ and plate $\mathcal{P}$ are of the same order i.e. $\omega'_b/\omega_p = O(1)$, one obtains the following condition:

$$\frac{G_b\mathcal{I}_b}{\rho_b J_b L'^2} = O\left(\frac{E'_p d^2}{\rho_p D^4}\right) \quad \text{i.e.} \quad \frac{G_b\rho_p}{E'_p\rho_b} = O\left(\frac{d^2L'^2}{D^4}\right) = O\left(\frac{\epsilon_p^2}{\varepsilon^2}\right) \tag{26}$$

In addition, we have to express the condition of asymmetric coupling stating that the action exerted by the plate on the beam acts as an external load. Thus, considering the balance in torsion along $\underline{a}_1$ (the torque is denoted $\mathcal{M}_b$ in $\mathcal{B}$), we have

$$\partial_{x_1}\mathcal{M}_b = O(M_p) \quad \text{i.e.} \quad O\left(\frac{\mathcal{M}_b}{L'}\right) = O(M_p)$$

where $\mathcal{M}_b = G_b\mathcal{I}_b\partial_{x_1}\theta = O(G_b l^4\frac{\theta}{L'})$ and $M_p = O(E'_p I_p\partial^2_{x_2}w) = O(E'_p\frac{d^3}{12}\frac{w}{D^2})$. Furthermore the kinematic variables of torsion and bending are related by $\theta = O(w/D)$. Thus we obtain a second condition

$$\frac{G_b l^4}{DL'^2} = O\left(\frac{E'_p d^3}{D^2}\right) \quad \text{i. e.} \quad O\left(G_b\epsilon_b^4\right) = \varepsilon^2 O\left(E'_p\epsilon_p^3\right) \tag{27}$$

In the case of an heterogeneous ribbed plate where $\epsilon_b = l/L = d/D = \epsilon_p = \epsilon$, (and then $\varepsilon = D/L = d/l$) conditions (26) and (27) are fulfilled when

$$\frac{E'_p\rho_b}{G_b\rho_p} = O\left(\frac{\varepsilon^2}{\epsilon^2}\right) \quad ; \quad \frac{E'_p}{G_b} = O\left(\frac{\epsilon}{\varepsilon^2}\right) \tag{28}$$

In the case of an homogeneous ribbed plate where $E_p = E_b$, $\rho_p = \rho_b$, (26) and (27) impose that

$$\frac{d}{D} = O\left(\frac{D}{L}\right) = O\left(\frac{l^{4/3}}{L^{4/3}}\right) \tag{29}$$

The conditions of inner resonance in torsion (26) and (27) differ from that established in bending (1)–(3). This reflects the fact that the beam bending rigidity is much lower (by a factor ϵ_b^2) that its torsional rigidity and consequently, for a beam of a given length, the fundamental frequency in bending and torsion differs by a factor ϵ_b. Nevertheless, in infinite (or sufficiently long) ribbed plates both inner resonance in bending and torsion can occur but they will involve different wavelengths in the beam.

5.1. Derivation of the torsional behavior of ribbed plates

In the same way as for the study in bending, the analysis in torsion is performed by assuming that the conditions (26) and (27) are satisfied. The developments are very similar, and then only the key points will be presented.

First, the asymptotic model of the beam $\mathcal{B}$ loaded in torsion reads

$$\begin{cases} \partial_{x_1}\mathcal{M}^{\mathcal{B}} + \displaystyle\int_{\Gamma_b} y_2\sigma_{S32}.n_2 - \int_{\Gamma_b} y_3\sigma_{S22}.n_2 = -\rho_b J_b\omega^2\theta(x_1) \\ \mathcal{M}^{\mathcal{B}} = G_b\mathcal{I}_b\partial_{x_1}\theta(x_1) \end{cases} \tag{30}$$

where the two integral terms in (30) account for the action of the plate on the beam and n_2 is the component of the outgoing normal of the beam section and takes the value ± 1 on $\Gamma_b^{\pm}$.

Second, the plate $\mathcal{P}$ in bending is described by the set (9). In the condition of scale separation (10), the description reduces to (11) except for the boundary conditions. Here the proper boundary conditions express that (i) at the leading order, the beam section undergoes a rigid body motion so that Γ_b^- and Γ_b^+ follows the same rotation $\theta(x_1)$, and (ii) since $l \ll D$, the vertical motion at the beam/plate interface is $O(\theta l)$ that is negligible compared to the plate deflection $W = O(\theta D)$. Thus, the plate problem reads now

$$\text{in } \mathcal{P} \quad \begin{cases} \partial_{x_2}T^{\mathcal{P}} = -\Lambda_p\omega^2 W \\ \partial_{x_2}M^{\mathcal{P}} - T^{\mathcal{P}} = 0 \\ M^{\mathcal{P}} = -E'_p I_p\partial^2_{x_2}W \end{cases} \qquad \text{on } \Gamma_p \quad \begin{cases} \forall x_1 \\ W(x_1, x_{2|\Gamma}) = 0 \\ \partial_{x_2}W(x_1, x_{2|\Gamma}) = \theta(x_1) \end{cases} \tag{31}$$

The solution of this linear problem in which rotation $\theta(x_1)$ is the forcing term takes the form $W(x_1,x_2) = D\theta(x_1)\psi(x_2)$ where $\psi_\omega(x_2)$ is the frequency dependent solution of

$$\partial^4_{x_2}\psi_\omega - \delta^4\psi_\omega = 0\,; \quad \psi_\omega(x_{2|\Gamma_p}) = 0\,; \quad \partial_{x_2}\psi_\omega(x_{2|\Gamma_p}) = 1/D$$

A standard resolution provides (recall that $\delta^4 = \Lambda_p\omega^2/(E'_p I_p)$ and $\delta^* = \delta D/2$)

$$\psi_\omega(x_2) = \frac{\sinh(\delta x_2)\sin(\delta^*) - \sin(\delta x_2)\sinh(\delta^*)}{2\delta^*(\cosh(\delta^*)\sin(\delta^*) - \cos(\delta^*)\sinh(\delta^*))} \quad ; \quad -D/2 < x_2 < D/2 \tag{32}$$

Infinite motion arises when the denominator of $\psi_\omega(x_2)$ vanishes. This happens at the eigenfrequencies of the antisymmetric modes of the plate (note that $\langle\psi_\omega\rangle = 0$). In accordance with the antisymmetric boundary conditions, the symmetric modes do not participate to the forced motion ψ_ω. It is useful for the following to introduce the quantities $\langle\frac{x_2}{D}\psi_\omega\rangle$ and $D^3\partial^3_{x_2}\psi_{\omega|\frac{D}{2}}$:

$$J^*_\omega = \left\langle\frac{x_2}{D}\psi_\omega\right\rangle = \frac{1}{D}\int_{-D/2}^{D/2}\frac{x_2}{D}\psi_\omega(x_2)\mathrm{d}x_2 = \frac{1}{(2\delta^*)^2}\frac{\coth(\delta^*)+\cot(\delta^*)-2/\delta^*}{\coth(\delta^*)-\cot(\delta^*)} \tag{33}$$

$$C^*_\omega = D^3\partial^3_{x_2}\psi_{\omega|\frac{D}{2}} = (2\delta^*)^2\ \frac{\coth(\delta^*)+\cot(\delta^*)}{\coth(\delta^*)-\cot(\delta^*)} \tag{34}$$

The beam/plate coupling is derived from the stress continuity $\underline{\underline{\sigma}}^{\mathcal{B}}.\underline{a}_2 = \underline{\underline{\sigma}}^{\mathcal{P}}.\underline{a}_2$ and the periodicity that provides $\sigma_{S22|\Gamma_b^\mp} = \sigma_{p22|\Gamma_p^\pm}$ and $\sigma_{S23|\Gamma_b^\mp} = \sigma_{t23|\Gamma_p^\pm}$. Then the action of the plate on the beam defined in (30) reads:

$$\int_{\Gamma_b} y_2\sigma_{S32}.n_2 = \int_{\Gamma_b^+}\frac{b}{2}\sigma_{S23} - \int_{\Gamma_b^-}-\frac{b}{2}\sigma_{S23} = \frac{b}{2}\left(\int_{\Gamma_p^-}\sigma_{t23} + \int_{\Gamma_p^+}\sigma_{t23}\right) = \frac{b}{2}\left(T^{\mathcal{P}}_{|\Gamma_p^-} + T^{\mathcal{P}}_{|\Gamma_p^+}\right) \tag{35}$$

$$-\int_{\Gamma_b} y_3\sigma_{S22}.n_2 = -\int_{\Gamma_b^+} y_3\sigma_{S22} + \int_{\Gamma_b^-} y_3\sigma_{S22} = -\int_{\Gamma_p^-} y_3\sigma_{p22} + \int_{\Gamma_p^+} y_3\sigma_{p22} = -M^{\mathcal{P}}_{|\Gamma_p^-} + M^{\mathcal{P}}_{|\Gamma_p^+} \tag{36}$$

Hence, the effective moment acting on the beam includes (i) the moment due to the sum of the shear efforts on the two sides of the plate and (ii) the differential moment between each side. Now, from the plate Eq. (31) we have on the one hand

$$\int_{-D/2}^{D/2} x_2\partial_{x_2}T^{\mathcal{P}}\mathrm{d}x_2 = -\Lambda_p\omega^2\int_{-D/2}^{D/2}x_2 W\mathrm{d}x_2 = -\Lambda_p D^3\langle\frac{x_2}{D}\psi_\omega\rangle\omega^2\theta(x_1) \tag{37}$$

and on the other hand, using integration by part

$$\int_{-D/2}^{D/2} x_2\partial_{x_2}T^{\mathcal{P}}\mathrm{d}x_2 = \int_{-D/2}^{D/2}\partial_{x_2}(x_2T^{\mathcal{P}})\mathrm{d}x_2 - \int_{-D/2}^{D/2}T^{\mathcal{P}}\mathrm{d}x_2 = \frac{D}{2}(T^{\mathcal{P}}_{|\Gamma_p^+} + T^{\mathcal{P}}_{|\Gamma_p^-}) - \int_{-D/2}^{D/2}\partial_{x_2}M^{\mathcal{P}}\mathrm{d}x_2$$

Thus, transforming the last integral, one obtains

$$M^{\mathcal{P}}_{|\Gamma_p^+} - M^{\mathcal{P}}_{|\Gamma_p^-} = \frac{D}{2}(T^{\mathcal{P}}_{|\Gamma_p^+} + T^{\mathcal{P}}_{|\Gamma_p^-})| + \Lambda_p D^3\langle\frac{x_2}{D}\psi_\omega\rangle\omega^2\theta(x_1) \tag{38}$$

then, observing that $T^{\mathcal{P}}_{|\Gamma_p^+} = T^{\mathcal{P}}_{|\Gamma_p^-} = -E'_pI_p\partial^3_{x_2}\psi_{\omega|\frac{D}{2}}D\theta(x_1)$

$$\int_{\Gamma_b} y_2\sigma_{S32}.n_2 - \int_{\Gamma_b} y_3\sigma_{S22}.n_2 = \left(-E'_pI_p(D+b)D\partial^3_{x_2}\psi_{\omega|\frac{D}{2}} + \Lambda_pD^3\langle\frac{x_2}{D}\psi_\omega\rangle\omega^2\right)\theta(x_1)$$

5.2. Homogenized torsional model of ribbed plates

The previous expression reported in (30) provides the effective torsional modeling. It involves the beam rotation $\theta(x_1)$ as the unique kinematic descriptor. To sum up we are lead to the following synthetic dual homogenized formulation

- the case where the beam is active $\theta(x_1)\neq 0$ gives the global modes associated with the non conventional effective beam/plate rotational inertia - that includes the static rotational inertia of the beam and the frequency-dependent effective rotational inertia of the plate - and a frequency-dependent torsional spring rigidity. This situation actually describes a co-dynamic beam/plate regime and the corresponding equation for the beam rotation $\theta(x_1)$ reads:

$$G_b\mathcal{I}_b\partial^2_{x_1}\theta = -\omega^2\left(\rho_bJ_b + \Lambda_pD^3J^*_\omega\right)\theta + \frac{E'_pI_p(D+b)}{D^2}C^*_\omega\theta \tag{39}$$

  where the frequency dependent parameters J^*_ω and C^*_ω of the plate are defined in (33) and (34) as:

$$J^*_\omega = \frac{1}{(2\delta^*)^2}\frac{\coth(\delta^*)+\cot(\delta^*)-2/\delta^*}{\coth(\delta^*)-\cot(\delta^*)} \quad ; \quad C^*_\omega = (2\delta^*)^2\ \frac{\coth(\delta^*)+\cot(\delta^*)}{\coth(\delta^*)-\cot(\delta^*)}$$

- furthermore, the above analysis in torsion assumes that the beams are rotating. However, if the beam stays at rest, i.e. $\theta(x_1) = 0$, vibrations of the plate are nonetheless possible. The latter are ruled by (9) together with the clamped conditions on Γ_p, and correspond to the guided waves with passive beams already described by (19). Note that to insure the vanishing of the torques exerted on both faces of the beam the motions are alternatively W and $-W$ from a plate to the adjacent one.

The governing equation associated with torsional waves (39) is non-conventional. Indeed, meanwhile J^*_ω and C^*_ω appear as an effective rotational inertia and rigidity they both are elasto-inertial parameters resulting from the elasto-dynamic regime in the plate and both present strong frequency variations with singularities. It can be established from expressions (33) and (34) that:

- $J^*_\omega \to -\frac{1}{60}$ when $\delta^*\to 0$ (hence $\omega\to 0$). Therefore the contribution of the quasi-statically bended plate to the rotational inertia is *negative* and takes the value $-\frac{1}{5}\frac{\Lambda_pD^3}{12}$,
- $C^*_\omega \to 12$ when $\delta^*\to 0$. Thus, the quasi-statically bended plate exerts an actual *return torque* corresponding to a torsional spring rigidity of *positive* value $\frac{12E'_pI_p(D+b)}{D^2}$,
- J^*_ω and $C^*_\omega \to \pm\infty$ when $\tan(\delta^*) = \tanh(\delta^*)$ i. e. at the eigenfrequencies $\{\omega_{tn}\}$ of the antisymmetric modes. When $\omega\to\omega^-_{tn}$ (resp. ω^+_{tn}), J^*_ω and $C^*_\omega \to -\infty$ (resp. $+\infty$),
- $J^*_\omega = 0$ when $\coth(\delta^*)+\cot(\delta^*) = 2/\delta^*$. This occurs at frequencies ω_{t_0n} that can be assessed as $\omega_{t_0n}\approx(2n+\frac{3}{2})^2\left(\frac{\pi}{D}\right)^2\sqrt{\frac{E_pI_p}{\Lambda_p}}$ (which are very close to $\omega_{s(n+1)}$ for $n>1$). Thus, in the intervals $[\omega_{t_0n},\omega_{tn}]$ the effective rotational inertia of $\mathcal{P}$ is *negative*.
- $C^*_\omega = 0$ when $\tanh(\delta^*)+\tan(\delta^*) = 0$, i.e. at the eigenfrequencies ω_{sn} of the symmetric modes. Thus in the intervals $[\omega_{sn},\omega_{tn}]$ the apparent torsional spring rigidity of the plate $\mathcal{P}$ is *negative*, which means that, instead of exerting a return torque, the bended plate exerts a repulsive torque.

The features of J^*_ω and C^*_ω are illustrated respectively in Figs. 4 and 5 with two values of structural damping. These terms normalized by their static values are also plotted in Fig. 6. These figures clearly highlight the strong frequency dependence and the singularities of both J^*_ω and C^*_ω at the eigenfrequencies $\{\omega_{tn}\}$, as well as their negative and positive static values respectively. Note that in between the singularities the fluctuations of the torsional spring rigidity are significantly larger than that of the rotational inertia.

5.3. Dispersion features of torsional waves

The dispersion of torsional waves on the form $\theta(x_1) = \exp(i\kappa_\omega x_1)$ is determined by the wavenumber κ_ω. The latter is de-

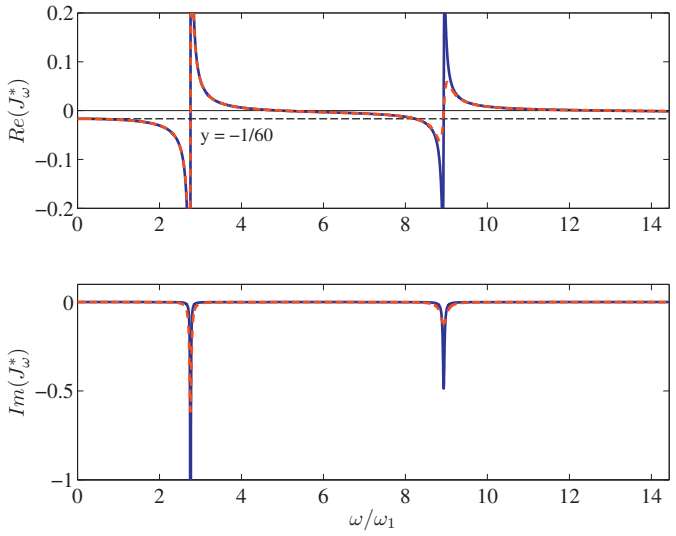

Fig. 4. Real an imaginary parts of the dimensionless apparent rotational inertia of the plate J^*_ω versus the dimensionless circular frequency ω/ω_{t1}; with structural damping $\eta = 0.5\%$ (—) , and $\eta = 2\%$ (— —).

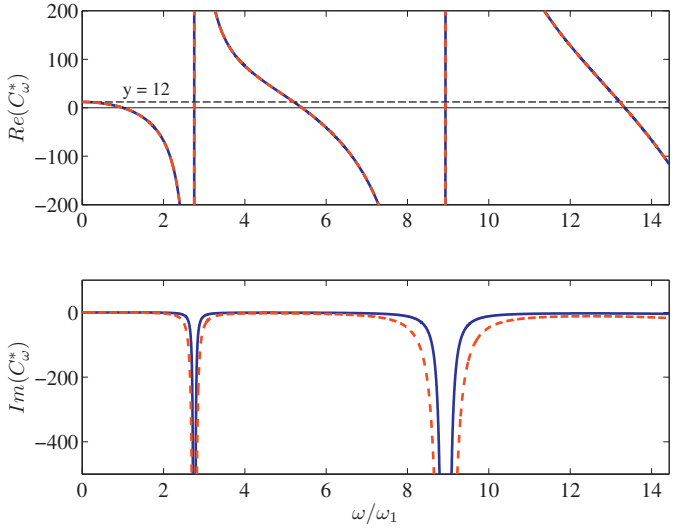

Fig. 5. Real an imaginary parts of the dimensionless the torsional spring rigidity of the plate C^*_ω versus the dimensionless circular frequency ω/ω_{t1}; with structural damping $\eta = 0.5\%$ (—) , and $\eta = 2\%$ (— —).

termined from (39):

$$\kappa^2_\omega = \frac{\omega^2\left(\rho_b J_b + \Lambda_p D^3 J^*_\omega\right) - \frac{E'_p I_p (D+b)}{D^2} C^*_\omega}{G_b \mathcal{I}_b} \tag{40}$$

Conversely to the classical non-dispersive torsional waves, the inner resonance of plate $\mathcal{P}$ reflected by the terms J^*_ω and C^*_ω induces a non-conventional dispersion. A full analysis of the properties would require the knowledge of the parameters due to the complex interaction between $J^*_\omega\omega^2$ and C^*_ω. Examples will be presented in Section 6. Nevertheless, one may notice that:

- when $\omega \to 0$ then $\kappa^2_\omega \to -12\frac{E'_p I_p (D+b)}{D^2 G_b \mathcal{I}_b} < 0$. Thus the torsional wavenumber is imaginary and the corresponding waves are *evanescent* from $\omega = 0$ to a cut-off frequency,
- significant dispersion effects are expected in the neighborhood of the eigenfrequencies of the *antisymmetric* modes. Furthermore, alternating frequency bands of evanescent or propagative waves will occur, corresponding to negative or positive values of κ^2_ω.
- at the eigenfrequencies of the *symmetric* modes $J^*_\omega \approx 0$ and $C^*_\omega = 0$. Consequently, the torsional wave in the ribbed plate should present features close to that of the propagative torsional wave in the beam alone.

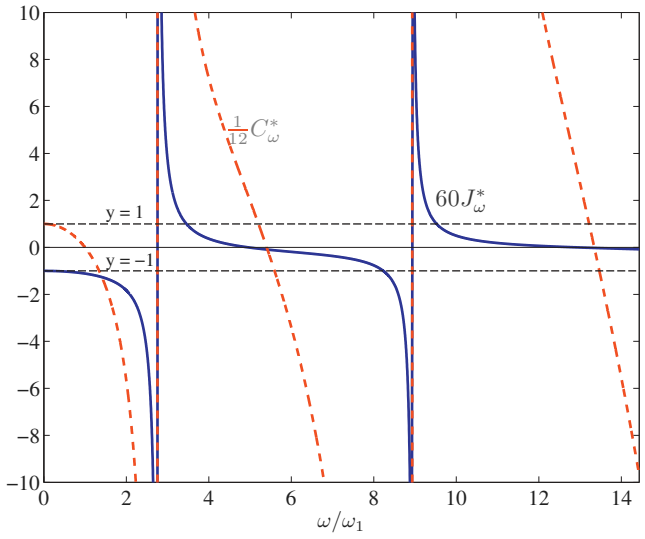

Fig. 6. Real parts of the normalized dimensionless apparent inertia of the plate $\langle \frac{x_2}{D}\psi_\omega \rangle$ (—), and normalized apparent torsional spring rigidity of the plate $D^3\partial^3_{x_2}\psi_{\omega|\frac{b}{2}}$ (— —) versus the dimensionless circular frequency ω/ω_{t1}.

The feature of the guided waves with passive beams were already described by (19). In fact, one may split the guided waves into those based on symmetric modes that are related to the flexural behavior, and those based on antisymmetric modes that are related to the torsional behavior.

Note finally that the validity of the homogenized model in torsion imposes (i) the classic restrictions on the reduced wavelengths in the beam and plate respectively $\mathcal{L}'_{\mathcal{B}_\omega} > l$ and $\mathcal{L}_{\mathcal{P}_\omega} > d$ that read:

$$\omega^2 < \text{Min}\left\{ \frac{G_b \mathcal{I}_b}{\rho_b J_b l^2} \, , \, \frac{E'_p I_p}{\Lambda_p d^4} \right\} \tag{41}$$

and (ii) the scale separation condition for the ribbed plate, i.e., $\kappa_\omega D < 1$, that corresponds to the frequencies ranges such that

$$\omega^2 < \frac{E'_p I_p (D+b) C^*_\omega + G_b \mathcal{I}_b}{\left(\rho_b J_b + \Lambda_p D^3 J^*_\omega\right) D^2} \tag{42}$$

Modeling (40) with active beams requires both conditions (41) and (42), while modeling (19) with passive beams and guided waves requires simply that $\omega^2 < \frac{E'_p I_p}{\Lambda_p d^4}$.

6. Examples, comparisons, discussion

In this section, the phenomena above described by the homogenized model constituted by the set of Eqs. (18)-(19)-(39) are illustrated on two realistic examples. One focuses first on the wave propagation along the beam axis in infinite ribbed plates. The dispersion relations are calculated according to the up-scaled model, and compared with a numerical approach. Second, we perform modal analysis on a ribbed plate of finite length. The co-dynamic conditions are specified in concrete terms, and the homogenized

Table 1
Mechanical properties and geometrical parameters of plates under study.

	E, ν	ρ (kg.m^{-3})	Dimensions
$\mathcal{R}_1$			
Beam $\mathcal{B}_1$	69×10^9 Pa, 0.3	2700	$l=b=2.5$ cm
Plate $\mathcal{P}_1$	69×10^9 Pa, 0.3	2700	$D=18.78$ cm, $d=3.3$ mm
$\mathcal{R}_2$			
Beam $\mathcal{B}_2$	69×10^9 Pa, 0.3	2700	$l=b=1$ cm
Plate $\mathcal{P}_2$	3×10^9 Pa, 0.3	1200	$D=12.3$ cm, $d=1.8$ mm

model is used to the calculate the frequency response function of the considered ribbed plate.

6.1. Ribbed plates under study

The two ribbed plates under study are denoted $\mathcal{R}_1$ and $\mathcal{R}_2$. The ribbed plate $\mathcal{R}_1$ consists in beams $\mathcal{B}$ and plates $\mathcal{P}$ both made of aluminum, while in the ribbed plate $\mathcal{R}_2$ the beam $\mathcal{B}$ is made of aluminium and the plate $\mathcal{P}$ is made of perspex which much softer than aluminum. The mechanical and geometrical parameters are summarized in Table 1.

The eigenfrequencies $f_l=\omega_l/(2\pi)$ of the three first symmetric and antisymmetric modes of the plates $\mathcal{P}_1$ and $\mathcal{P}_2$ are

$$f_{s1}=519\ ;\ f_{t1}=1432\ ;\ f_{s2}=2808\ ;\ f_{t2}=4641\ ;\ f_{s3}=6934$$
$$f_{t3}=9685\ \text{Hz}\quad \text{for}\quad \mathcal{R}_1$$

$$f_{s1}=208\ ;\ f_{t1}=573\ ;\ f_{s2}=1123\ ;\ f_{t2}=1857\ ;\ f_{s3}=2774\ ;$$
$$f_{t3}=3874\ \text{Hz}\quad \text{for}\quad \mathcal{R}_2$$

From the values given in Table 1, the effective parameters and the wavenumbers are calculated for $\mathcal{R}_1$ and $\mathcal{R}_2$ (a structural damping coefficient $\eta=0.5\%$ is considered). A detailed analysis is presented here-below for $\mathcal{R}_1$ and, to save place, only synthetic results are given for $\mathcal{R}_2$.

6.2. Analysis of wave dispersion of ribbed plates $\mathcal{R}_1$

To perform the analysis, it is convenient to split the waves involving the symmetric and antisymmetric modes. In doing so one eases the understanding of the underlying mechanisms (i) of the flexural waves and symmetric guided waves and (ii) of the torsional waves and antisymmetric guided waves. Hence, the flexural (respectively torsional) waves is concurrently commented with the symmetric (respectively antisymmetric) guided waves.

6.2.1. Waves involving symmetric modes

Symmetric modes are involved in both the bending waves with active beam and the symmetric guided wave with passive beam.

The real and imaginary parts of the flexural wavenumber in the active beam regime (20) versus frequency – in the range of the first two symmetric eigenmodes of the plate $\mathcal{P}_1$ –are drawn in Fig. 7. One observes that:

- in the low frequency domain, the wavenumber matches that of the beam $\mathcal{B}$ whose static linear mass would be replaced by that of the ribbed plate. Actually, the static linear mass of the whole ribbed plate is retrieved when $\omega=0$, see (18),
- significant un-conventional dispersion is observed around the eigenfrequencies f_{s1} and f_{s2} of the symmetric modes of $\mathcal{P}$. In the frequency bands corresponding to negative effective linear mass $\Lambda_{eff}=\Lambda_b+\Lambda_p D\langle\phi_\omega\rangle$, the real and imaginary parts of the wavenumber are (quasi)-identical (the difference relies on the slight damping factor considered). Consequently, the bending wave is strongly damped,

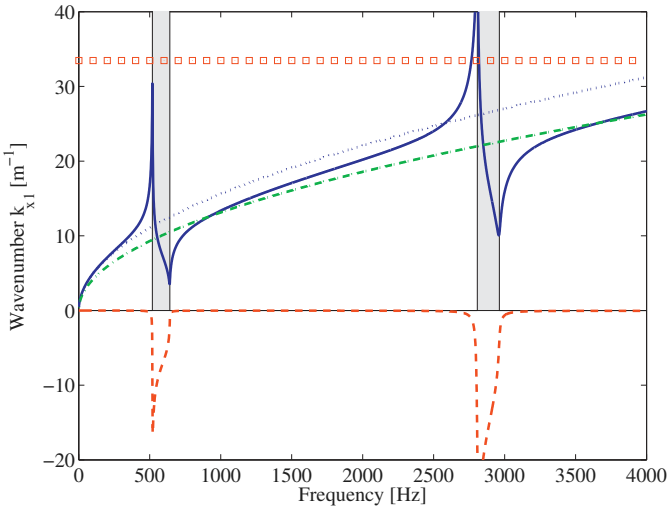

Fig. 7. Bending wavenumber along the beam axis of the ribbed plate $\mathcal{R}_1$ derived from (18), (real part (—) and imaginary part (– –)). For comparison the bending wavenumbers of the beam $\mathcal{B}$ itself (—·), and of the beam with the static lineic mass of the ribbed plate (···) are also plotted. The frequency bands of negative effective lineic mass are indicated by the shadowed zones (▬). The maximum value of the wavenumber for the validity of the beam model itself in bending (□).

- in the close vicinity of f_{s1} and f_{s2}, the waves are almost not damped and present either a velocity much lower than that of the beam with the whole mass (lower bound) or a velocity much larger – say up to three times – than the velocity of the beam itself (upper bound). Note also that outside of the bands of unconventional dispersion, as the frequency increases, the wavenumber tends to that of the beam alone $\mathcal{B}$, due to the reduction of modal mass of the plate $\mathcal{P}$ (actually, outside of the resonance frequency bands the effective linear mass of plate $\mathcal{P}$ vanishes as the frequency increases)

In Fig. 8, the wavenumbers of the symmetric guided waves calculated from approximated formulae (22) and (23) are displayed.

As indicated by the theory, the cut-off frequencies are the eigenfrequencies f_{s1} and f_{s2} of the symmetric modes of the plate. Below the cut-off frequencies the wavenumbers are purely imaginary (resp imaginary or complex) when estimated by (22) (resp. (23)) whereas they both are purely real above the cut-off frequencies and leads to propagating waves. In order to check the relevancy of the two approaches the results of finite element numerical computation (as described in Section 6.2.3) are also displayed. It appears that (23) fits better the numerical results.

6.2.2. Waves involving antisymmetric modes

Antisymmetric modes are mobilized in the torsional waves with active beam and in the antisymmetric guided waves with passive beam.

The real and imaginary parts of the torsional wavenumber in the active beam regime (40) is plotted in the [0–4 kHz] frequency range in Fig. 9. It appears that:

- on the whole frequency range, due to the contribution of the bended plate $\mathcal{P}$, the torsional wave dispersion of the ribbed plate strongly differs from that of the beam $\mathcal{B}$ alone,
- several bands (shadowed zones in Fig. 9) of imaginary wavenumber appear, the first one at low frequency, the next ones after the eigenfrequency f_{tn} of the antisymmetric modes of the plate $\mathcal{P}$. They correspond to evanescent torsional waves,

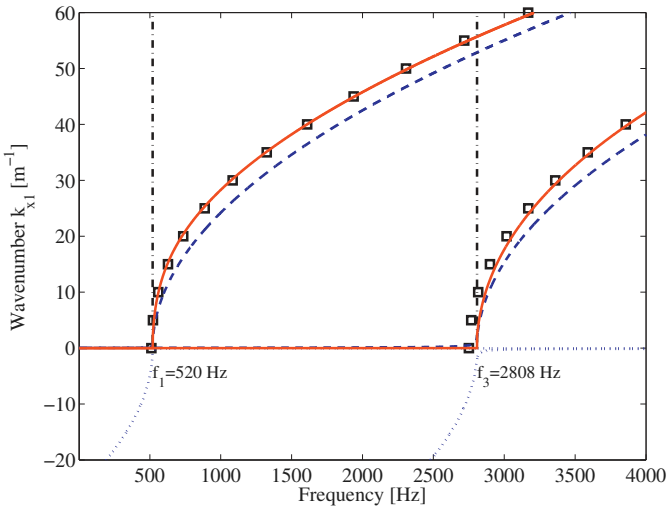

Fig. 8. Wavenumbers of the symmetric guided waves of the ribbed plate $\mathcal{R}_1$ derived from (22) (real part (— —) and imaginary part (. . .)) and from (23) (real part —). The eigenfrequencies of the symmetric eigenmodes of the plate $\mathcal{P}$ are indicated by vertical dotted lines. For comparison, finite element computation of the symmetric guided waves wavenumbers (□).

- out of the evanescent zones, a strong un-conventional dispersion is observed with singularities at the eigenfrequencies of the antisymmetric modes f_{tn}.

In Fig. 10, the wavenumbers calculated from (22) and (23) of the antisymmetric guided waves are displayed. The same comments than those made for the made for symmetric guided waves apply, the cut-off frequencies being here given by the eigenfrequencies f_{tn} of the antisymmetric modes. Remark that the successive branches of the guided waves are alternatively associated with symmetric and antisymmetric modes.

6.2.3. Comparison with numerical approaches of dispersion

For comparison with the theoretical approach, the ribbed plate $\mathcal{R}_1$ has been investigated numerically in the framework of the Floquet-Bloch method. The latter explicitly accounts for the periodicity of the cell to extract its propagation characteristics.

The modeled unit cell Ω consists in a thin slice of depth Δ depicted in Fig. 11. The cell is described through a three-dimensional finite element model. Phase shift conditions are imposed on the opposite faces of the unit cell as $u_b = \exp(-jk_{x_1}\Delta)u_f$ where u_f and u_b are the displacements of forward and backward part of the cell, k_{x_1} is the wavenumber along the $\underline{a}_1$ direction. For a given frequency, the dynamic balance formulated from the stiffness and mass matrices yields an eigenvalue problem whose resolution enables to track the various dispersion branches. The implementation of the eigenvalue problem is performed using the Wave Finite Element Method (Ichchou et al., 2008b) improved by modal reduction (Zhou et al., 2015) and (Droz et al., 2014) denoted hereafter CWFEM (Condensed Wave Finite Element Method). Note that for clear identification of guided waves, we defined specific phase shift conditions corresponding to a plate having two opposites sides at rest. The computed dispersion diagram of the waves propagating waves along $\underline{a}_1$ is presented in Fig. 12. One notices

- two linear branches that correspond to the *in-plane* shear and compressional modes which are not dispersive (in the frequency range under study). Their wavenumbers are classically given by the mean values of the modulus and density of the beam $\mathcal{B}$ and the plate $\mathcal{P}$. Namely $k_c = \omega\sqrt{\frac{\overline{\rho}}{\overline{\mu}}}$ and $k_s = \omega\sqrt{\frac{\overline{\rho}}{\overline{E}}}$ respectively, where $\overline{E} = (E_b bl + E'_p dD)/S$, $\overline{\mu} = (\mu_b bl + \mu_p dD)/S$, $\overline{\rho} = (\rho_b bl + \rho_p dD)/S$, $S = bl + dD$.

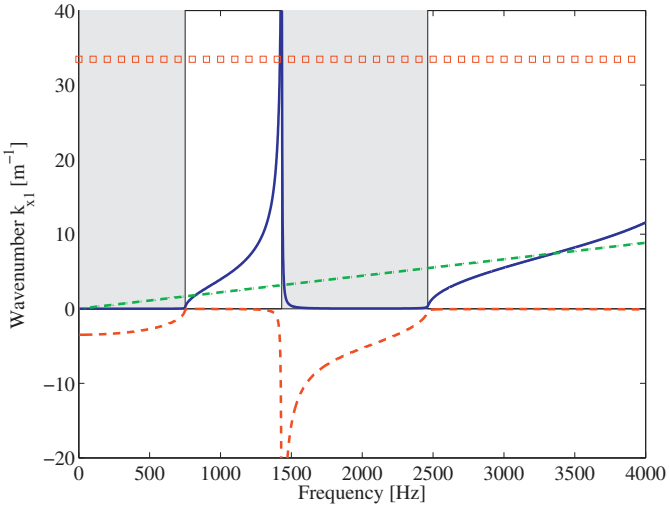

Fig. 9. Wavenumber of the torsional wave (real part (—) and imaginary part (— —)) and of the first antisymmetric guided waves (. . .). For comparison, the torsional wavenumbers of the beam $\mathcal{B}$ itself are also plotted (— .). The shadowed zones corresponds to the frequency bands of negative effective torsional inertia (▬). The maximum value of the wavenumber for the validity of the beam model itself in bending (□).

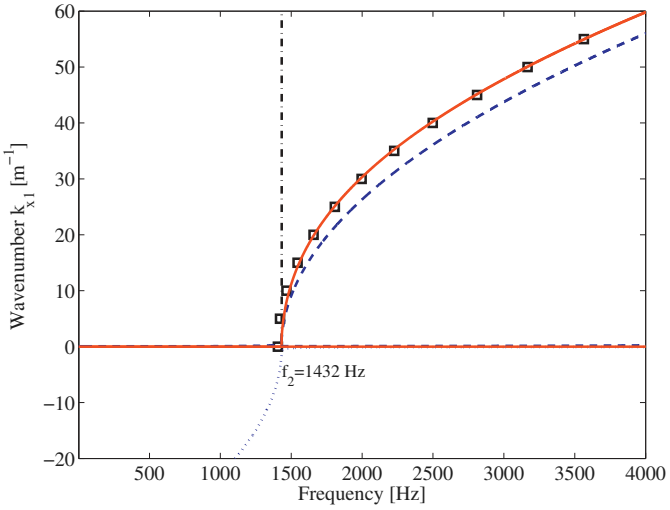

Fig. 10. Wavenumbers of the antisymmetric guided waves of the ribbed plate $\mathcal{R}_1$ derived from (22) (real part (— —) and imaginary part (. . .)) and from (23) (real part —). The eigenfrequencies of the antisymmetric eigenmodes of the plate $\mathcal{P}$ are indicated by vertical dotted lines. For comparison, finite element computation of the antisymmetric guided waves wavenumbers (□).

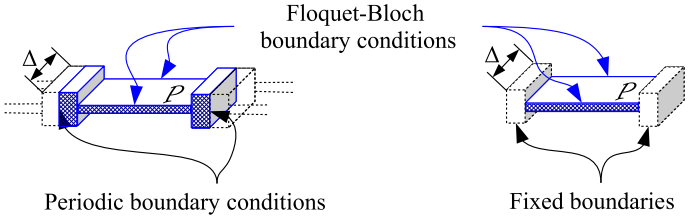

Fig. 11. Periodic cell of ribbed plate considered for the computation of full dispersion diagram Fig. 12 (a), and for the computation of guided waves wavenumbers only Fig. 8,10 (b).

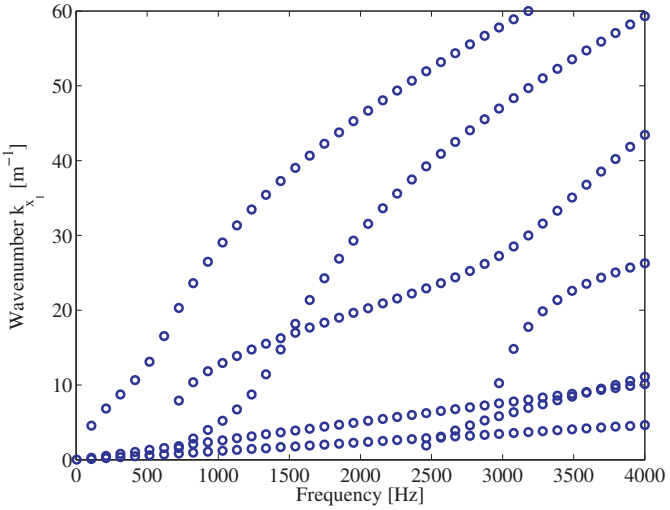

Fig. 12. Dispersion curves of the ribbed plate $\mathcal{R}_1$ computed through CWFEM (○).

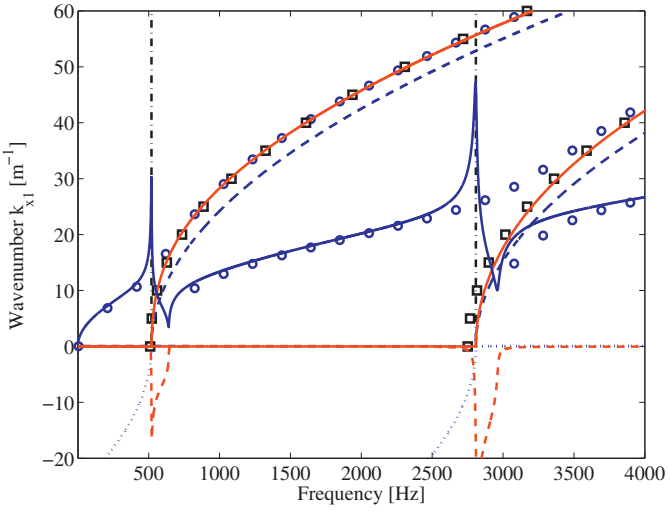

Fig. 13. Wavenumbers of the symmetric modes of propagation. Homogenized model that encompass inner resonance in bending (real part (—) and imaginary part (– –)) and guided waves (real part (– –) and imaginary part (. . .). CWFEM computation (○). Computation of the symmetric guided waves wavenumbers (□).

- other non linear branches corresponding to dispersive waves involving *out-of-plane* kinematics. However, the identification of the torsional or flexural nature of theses dispersive modes is not achievable from the dispersion curves only.

The Figs. 13 and 14 provide the theoretical/numerical comparison of the dispersion diagram associated with the symmetric and antisymmetric wave kinematics respectively. On both figures, one notices the good agreement between the numerical simulations and the wavenumbers given by the homogenized model with active or passive beams. The ribbed plate model ease the understanding of the dispersion features: the bending and torsional kinematics are clearly identified, as well as the transition between the different branches and the cut-on frequency of the guided waves corresponding to the eigenfrequencies of the plate. The activation of the torsional kinematics around 750 and 2460 Hz is also correctly predicted.

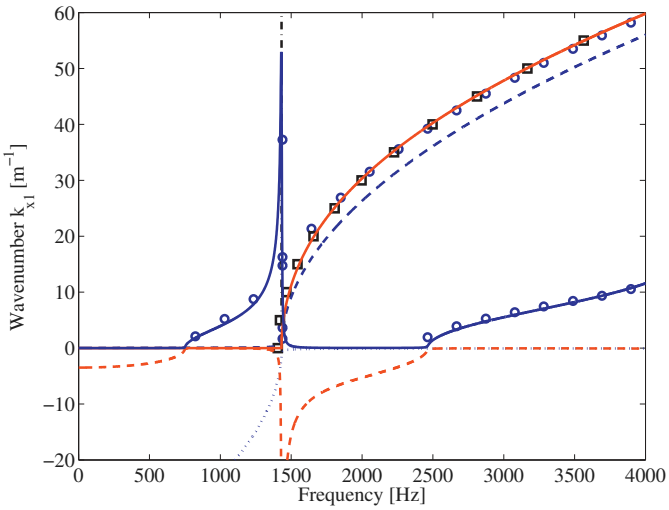

Fig. 14. Wavenumbers of the antisymmetric modes of propagation. Homogenized model that encompass inner resonance in torsion (real part (—) and imaginary part (– –)) and guided waves (real part (– –) and imaginary part (. . .)). CWFEM computation (○). Computation of the antisymmetric guided waves wavenumbers (□).

6.3. Wave dispersion of ribbed plate $\mathcal{R}_2$

The same analysis has been performed on the ribbed plate $\mathcal{R}_2$ (see Table 1). The comparison of the theoretical/numerical results displayed in Fig. 15 shows a good agreement. These two different examples $\mathcal{R}_1$ and $\mathcal{R}_2$ substantiate the validity and the robustness of the homogenized model.

6.4. Implementation of the homogenized model for finite ribbed plate

6.4.1. Further comments on the co-dynamic condition

Let us formulate more precisely the co-dynamic condition. As shown above the singular behavior of the ribbed plates is associated to the eigenmodes and frequency of the plate. Thus for a ribbed plate of finite size L, one may reach different co-dynamic situation according the considered mode for the beam and the plate.

For a ribbed plate clamped at its extremities, the size $\mathcal{L}_{nJ}$ such that the n^{th} symmetric mode of the plate arises at the same frequency than that of the J^{th} mode in *bending* of the beam can be assessed being expressing that $\omega_{sn} = \omega_J$. By definition:

$$\omega_{sn} = \delta_{\mathcal{P}}^2 \sqrt{\frac{E'_p I_p}{\Lambda_p}} \quad ; \quad \omega_J = \delta_{\mathcal{B}}^2 \sqrt{\frac{E_b I_b}{\Lambda_b}}$$

and, in accordance with the resonance states $\delta_{\mathcal{P}} D = (2n - 1/2)\pi$, $\delta_{\mathcal{B}} \mathcal{L}_{nJ} = (J + 1/2)\pi$. This yields

$$\mathcal{L}_{nJ} = D \frac{J + 1/2}{2n - 1/2} \sqrt[4]{\frac{E_b I_b \Lambda_p}{E'_p I_p \Lambda_b}}$$

The same reasoning enables to assess the size $\mathcal{L}'_{mK}$ such that the frequency ω_{tm} of the m^{th} antisymmetric mode of the plate coincides with the frequency of the K^{th} mode in *torsion* of the beam. In that case

$$\omega_{tm} = \delta_{\mathcal{P}}^2 \sqrt{\frac{E'_p I_p}{\Lambda_p}} \quad ; \quad \omega_K = \delta'_{\mathcal{B}} \sqrt{\frac{G_b \mathcal{I}_b}{\rho_b J_b}}$$

and, we have $\delta_{\mathcal{P}} D = (2m + 1/2)\pi$, $\delta'_{\mathcal{B}} \mathcal{L}'_{mK} = K\pi$, so that

$$\mathcal{L}'_{mK} = D \frac{K}{2m + 1/2} \sqrt[4]{\frac{E_b I_b}{\Lambda_b}} \sqrt{\frac{\rho_b J_b}{G_b \mathcal{I}_b}}$$

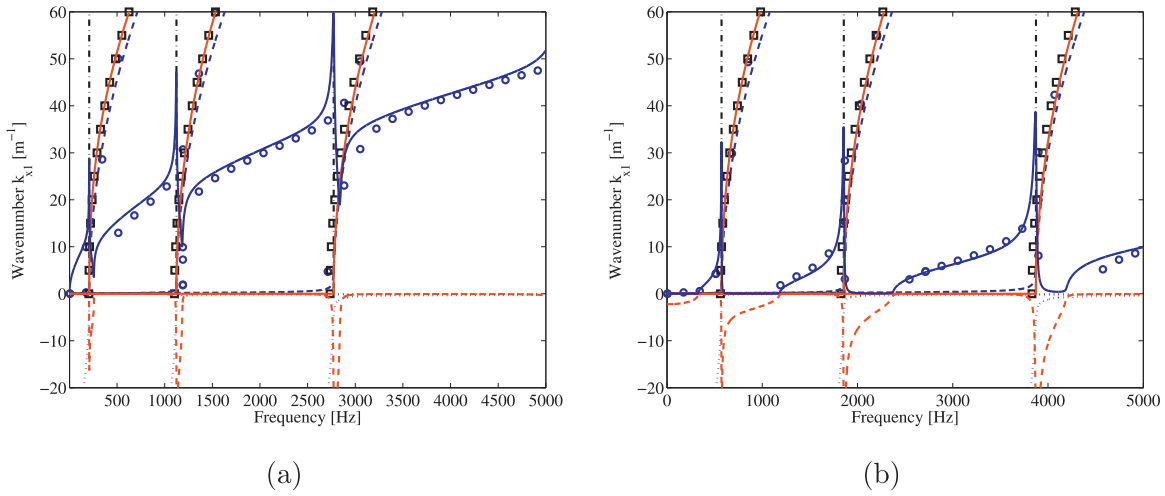

Fig. 15. (a) Wavenumbers of the symmetric modes of propagation. Homogenized model that encompass inner resonance in bending (real part (—) and imaginary part (– –)) ; (b) Wavenumbers of the antisymmetric modes of propagation. Homogenized model that encompass inner resonance in torsion (real part (—) and imaginary part (– –)). Guided waves (real part (– –) and imaginary part (. . .). CWFEM computation (○). Computation of the guided waves wavenumbers (□).

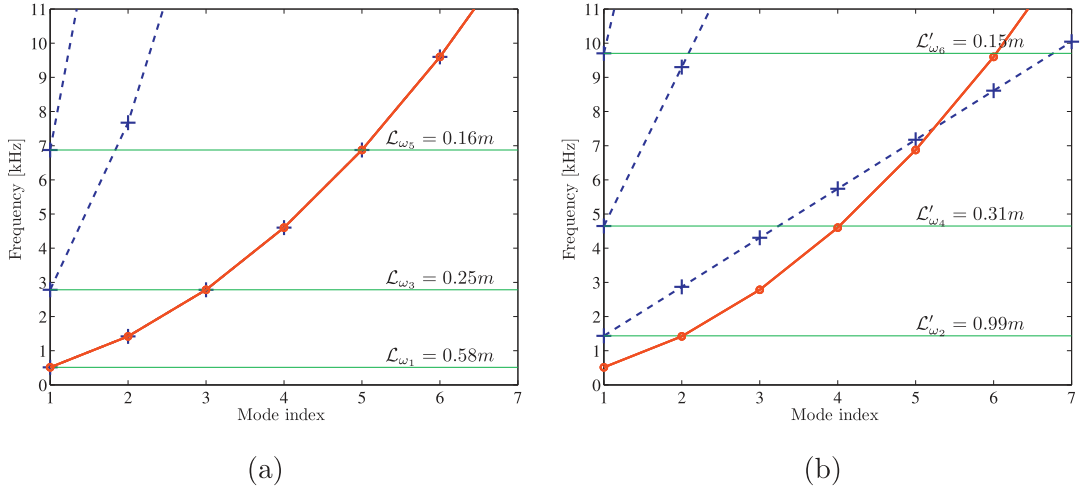

Fig. 16. Distribution of eigenfrequencies associated with the plate (— ○ —) and the beam (— + —) in bending (a) and torsion (b), with corresponding beam length suitable for co-resonance.

A graphical representation of the flexural and torsional co-resonance matching is given in Fig. 16 for the ribbed plate $\mathcal{R}_1$ clamped at its extremities. The indicated lengths correspond to $\mathcal{L}'_{n1}$, $\mathcal{L}'_{m1}$, $n, m = 1, 2, 3$ so that the fundamental mode of the beam coincide with a given mode of the plate. For instance, considering a plate of length $\mathcal{L}_{31}$, the co-resonance regime is reached at ω_{s3}. At frequencies $\{\omega_{s1}, \omega_{s2}\}$, the beam may undergoes a quasi-static regime however inner resonance appear in the plate. This will also be the case for antisymmetric modes at $\{\omega_{t1}, \omega_{t2}, \dots\}$ since the eigenfrequencies of the beam in torsion are much higher than in bending. Conversely, at frequencies ω_{sn}, $n > 3$ the beam undergoes a dynamic regime (not necessarily at resonance) and the plate resonates.

As a numerical example, considering a clamped ribbed plate $\mathcal{R}_1$ of length $L = 0.5$ m, the fundamental and higher eigenfrequencies in bending of the beam and the plate are close and occur at [519 ; 1432 ; 2808 ; 4641 ;...] Hz, while they significantly differ in torsion since the torsional resonance of the beam occur at [2840 ; 5680 ;...] Hz. Focusing on the fundamental bending mode, the five dimensionless parameters are $\{\epsilon_b = 0.05$; $\epsilon_p = 0.017$, $\varepsilon = 0.36$, $E_p/E_b = 1$, $\rho_b/\rho_p = 1\}$. Note that (i) the condition of asymmetric coupling (3) is satisfied since $\frac{E_b\epsilon_b^4}{E_p\epsilon_p^3} = 1.2 = O(1)$, and (ii) the dimensionless parameters are small enough to insure scale separation.

Symmetric modes enable to reach the co-dynamic condition in bending and leads to $\mathcal{L}_{\omega_{p;1,3,5}}$. Alternatively, antisymmetric modes yields the design for co-dynamic regime when the plate makes the beam rotate and yields $\mathcal{L}'_{\omega_{p;2,4,6}}$.

6.4.2. Frequency response functions of a finite ribbed plate

As an example of implementation of the homogenized model in bending (18) the frequency response functions (FRF) of the ribbed plate $\mathcal{R}_1$, of finite length 0.5 m, clamped at both extremities has been determined considering identical imposed harmonic displacements at the clamped extremities. The reference is taken

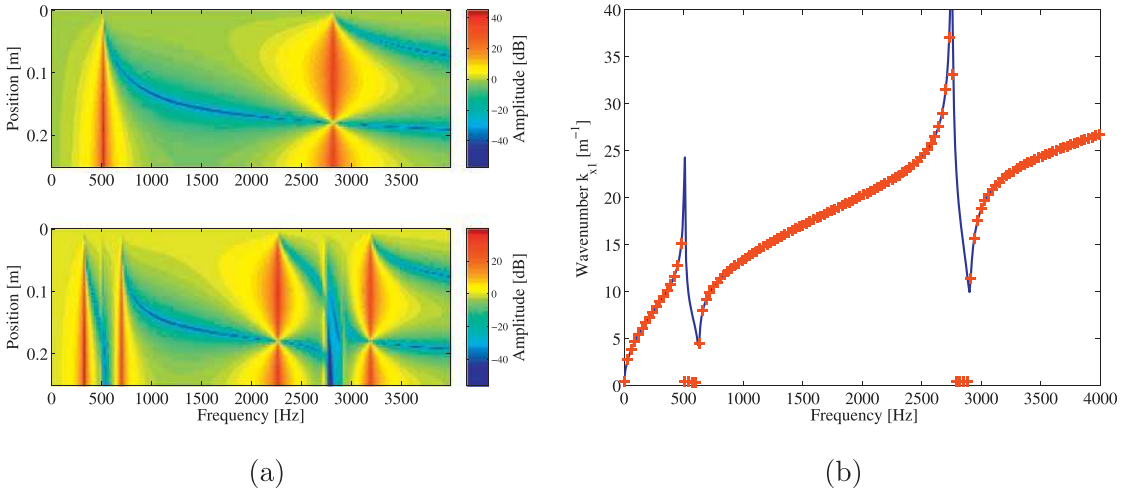

Fig. 17. (a) Two-dimensional representation of transfer functions calculated for the beam alone (top) and with the resonating plate (bottom). (b) Flexural wavenumber, analytical (—), reconstructed by IWC from theoretical FRFs (+). Calculation with clamped-clamped conditions.

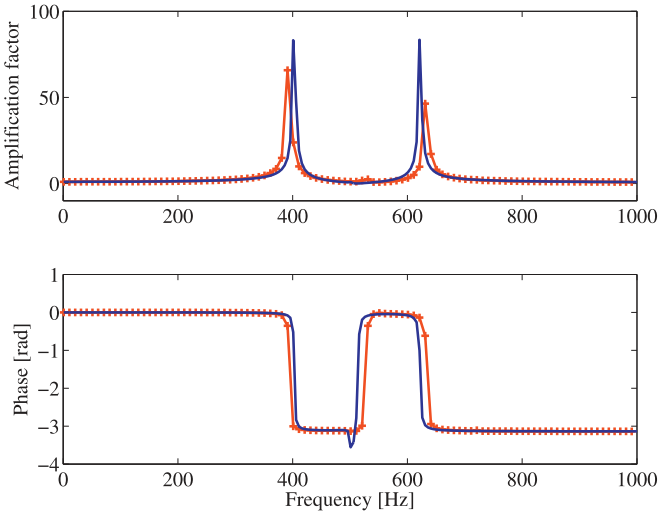

Fig. 18. Transfer function H on the ribbed plate with inner resonance : homogenized (— —), FEM (− + −).

onto the extremity while the receiver is located at any point along the beam. In order to show the effect of inner resonance, a two-dimensional representation of the FRFs is presented in Fig. 17. These analytical FRFs are plotted with respect to the receiver's position on the beam, (for its half-length only because of the symmetry). In absence of inner resonance, the symmetric modes resonance frequencies of the beam are identified as stripes around 519 and 2808 Hz. Accounting for the inner resonance effects leads to significant decrease of amplitude at those particular frequencies. Attenuation zones spread over the whole length of the beam except around $x = 0$, i.e. in the neighborhood of the excitation. The counterpart is the creation of two peaks on both sides of the anti-resonance. The dispersion curve associated with flexural waves in the beam affected by local resonance of the plate, as that presented in Fig. 7, can be recovered from these FRFs using the IWC (Inhomogeneous Wave Correlation) (Berthaut et al., 2005) and Mc Daniel (McDaniel and Shepard, 2000) methods. Such a processing is performed here on theoretical FRFs and illustrated in Fig. 17. Similar post-processing was achieved on experimental FRF's and will be published in a forthcoming paper.

Note that anti-resonances appear exactly at the beam eigenfrequencies since the same boundary conditions for the beam and the plate were considered to illustrate the case of co-resonance. Considering, for example, clamped-free boundary conditions with (18) would yield another distribution of eigenfrequencies and anti-resonances while band gaps associated with the plate would not change.

For consistency, an analytical forced response is compared with the computation in Fig. 18. For this comparison, the receiver is located at the half-length of the beam $x_r = 0.25$ m and the reference is taken onto the excitation point $x_e = 0$. The transfer function $H = U(x_r)/U(x_e)$ is plotted as the ratio of transverse displacements at the receiver's location and the excitation, two curves match correctly, and this preliminary comparison constitutes a promising result pending experimental validation.

7. Conclusion

Asymptotic homogenization applied to periodically ribbed plates allowed predicting their macroscopic behavior accounting for inner resonance resulting from contrasted geometrical parameters and/or mechanical properties. These contrasts lead to situations of co-resonance and asymmetric coupling between the plate and the beam. In this context, and within the scale separation assumption, the procedure yields an analytical homogenized model constituted by the set of equations (18)-(19)-(39) whose the effective parameters are fully determined from the knowledge of the mechanical and geometrical parameters of the plate and beam constituting the structure. The complex dynamic behavior is shown to encompass several mechanisms associated with enriched kinematics:

- for both flexural and torsional kinematics, one identifies two types of waves governed by two distinct differential equations that describes (i) waves where both beam and plate moves, and (ii) guided waves where the plate only is set in motion,
- the flexural waves with active beam are affected by the frequency dependent effective mass of the moving plate that takes positive or negative values. The consequence on the dispersion is to induce singularities associated with the symmetric eigenmodes. In particular, frequency bands of strong attenuation appear,

- the torsional waves with active beam are affected by both the effective rotational inertia and the torsional spring rigidity arising from the bended plate. Both of these contributions are frequency dependent and combine together so that the torsional wave also exhibit un-conventional dispersion with cutoff frequencies and attenuation zones associated with antisymmetric modes of the plate. Notably, at low frequencies only evanescent waves exist,
- the guided waves are alternatively related to the symmetric and antisymmetric modes of the moving plate and are propagative above the corresponding eigenfrequencies.

By principle, the WFE method is more versatile and general than the presented model well suited for ribbed plates. However, the interpretation of the WFE computed dispersion curves for this coupled physics problem is difficult and the presented model solves the problem by explaining in detail the origins and parameters controlling these curves. All the branches of the dispersion diagram are identified from the homogenized model and each of them is ruled by a specific dispersion equation established theoretically under an explicit form. Furthermore, the predictions of the homogenized model have been successfully compared to numerical calculations conducted using CWFEM method. Particularly, the homogenized model captures correctly the local resonances appearing on the flexural and torsional branches as well as cut-off frequencies of the torsional and guided waves.

The scale separation assumption, together with the coresonance matching and the asymmetric coupling can be reexpressed in terms of design rules to design ribbed plate panels having specific atypical features in a given frequency range.

Experimental validation has been performed and will be presented in a forthcoming publication. In addition, extensions to orthogonally-ribbed plates are in progress to describe cellular panels, as investigated e.g. in Varanasi et al. (2013), or membrane-type metamaterials.

Acknowledgments

This work was supported by the LabEx CeLyA (Centre Lyonnais d'Acoustique, ANR-10-LABX-0060) of Université de Lyon, within the program "Investissements d'Avenir" (ANR-11-IDEX-0007) operated by the French National Research Agency (ANR).

Appendix A. Derivation of the beam model

A1. Scaled formulation

The beam kinematics is constrained by the fact that tangential stress are negligible on $\partial S_b - \Gamma_b$. The normal vector associated with the contour ∂S_b is $\underline{n} = n_\alpha \underline{a}_\alpha$, thus:

$$\sigma_{1\alpha} n_\alpha = 0 / \partial S_b \qquad \text{with} \qquad \sigma_{1\alpha} = \mu(\partial_{x_\alpha} \tilde{u}_1 + \partial_{x_1} \tilde{u}_\alpha)$$

Since $\partial_{x_\alpha} \tilde{u}_1 = O(\tilde{u}_1/l)$ and $\partial_{x_1} \tilde{u}_\alpha = O(\tilde{u}_\alpha/L)$, the vanishing of tangential stress $\sigma_{1\alpha}$ on ∂S_b requires, for the components of $\tilde{u} = \tilde{u}_1 \underline{a}_1 + \tilde{u}_\alpha \underline{a}_\alpha$:

$$O\left(\frac{\tilde{u}_1}{l}\right) = O\left(\frac{\tilde{u}_\alpha}{L}\right) \qquad \text{so} \qquad O(\tilde{u}_1) = \epsilon_b O(\tilde{u}_\alpha)$$

Hence, the displacements along the axis are of a lower order compared to transverse displacements. Thus the displacements are normalized writing $u_1 = \epsilon_b u_1$ in such a way that $O(u_1) = O(u_\alpha)$:

$$\tilde{u} = \epsilon_b u_1 \underline{a}_1 + u_\alpha \underline{a}_\alpha \tag{A.1}$$

According to the beam geometry, the tensors of strains $\underline{\underline{e}}$ and stresses $\underline{\underline{\sigma}}$ split into three reduced tensors, as $\underline{\underline{A}} = A_N \underline{a}_1 \otimes \underline{a}_1 + (\underline{A}_T \otimes \underline{a}_1 + \underline{a}_1 \otimes \underline{A}_T) + \underline{\underline{A}}_S$ with $A_N = A_{11}$ is the axial stress or strain (scalar), $\underline{A}_T = A_{1\alpha} \underline{a}_\alpha$ are the section out-of-plane stress or strain (vector), $\underline{\underline{A}}_S = A_{\alpha\beta}(\underline{a}_\alpha \otimes \underline{a}_\beta + \underline{a}_\beta \otimes \underline{a}_\alpha)$ are the section in-plane stress or strain (tensor). The elastic linear isotropic constitutive law reads $\underline{\underline{\sigma}} = \lambda tr(\underline{\underline{e}}) + 2\mu \underline{\underline{e}}$, and denoting $\underline{\underline{I}}_S = \underline{e}_2 \otimes \underline{e}_2 + \underline{e}_3 \otimes \underline{e}_3$ the identity tensor in the section, the reduced stress tensors read:

$$\sigma_N = \lambda(tr(\underline{\underline{e}}_S) + e_N) + 2\mu e_N \qquad \underline{\sigma}_T = 2\mu \underline{e}_T$$
$$\underline{\underline{\sigma}}_S = \lambda(tr(\underline{\underline{e}}_S) + e_N)\underline{\underline{I}}_S + 2\mu \underline{\underline{e}}_S$$

The local governing equation consists in the momentum balance with body force $\underline{b}$ and contact force $\underline{f}$ ($\underline{f} = \underline{f}^+$ on Γ_b^+ and $\underline{f} = \underline{f}^-$ on Γ_b^-):

$$\underline{div}_y(\underline{\underline{\sigma}}) = \underline{b} \ \text{ in } \ S_b \qquad ; \qquad \underline{\underline{\sigma}}.\underline{n} = \begin{cases} 0 & \text{on } \partial S_b - \Gamma_b \\ \underline{f} & \text{on } \Gamma_b \end{cases} \tag{A.2}$$

Expressed in a two-scale form, (A.2) splits into a scalar balance along the length of the beam (along $\underline{a}_1$):

$$\frac{\partial \sigma_N}{\partial_{x_1}} + \epsilon_b^{-1} div_y(\underline{\sigma}_T) = b_1 \ \text{ in } \ S_b \quad ; \quad \underline{\sigma}_T.\underline{n} = \begin{cases} 0 & \text{on } \partial S_b - \Gamma_b \\ f_1 & \text{on } \Gamma_b \end{cases} \tag{A.3}$$

and a vectorial balance in the section plane (in the $(\underline{a}_2, \underline{a}_3)$ plane):

$$\frac{\partial \underline{\sigma}_T}{\partial_{x_1}} + \epsilon_b^{-1} \underline{div}_y(\underline{\underline{\sigma}}_S) = b_\alpha \underline{a}_\alpha \ \text{ in } \ S_b \quad ; \quad \underline{\underline{\sigma}}_S.\underline{n} = \begin{cases} \underline{0} & \text{on } \partial S_b - \Gamma_b \\ f_\alpha \underline{a}_\alpha & \text{on } \Gamma_b \end{cases} \tag{A.4}$$

In order to satisfy the separation of scales, loading terms $\underline{b}$ and $\underline{f}$ must be introduced at orders $b_1 = \epsilon_b b_1^1, b_\alpha = \epsilon_b^2 b_\alpha^2, f_1 = \epsilon_b^2 f_1^2, f_\alpha = \epsilon_b^3 f_\alpha^3$. Consequently, the three first problems related to the local balance are the same as in the static unloaded case. In dynamics, the body force term $\underline{b}$ in (A.2) reads $\underline{b} = -\rho\omega^2 \underline{u}$ where the axial component is held by u_1^1 and the transverse component is held by u_α^0, so that $b_1^1 = -\rho\omega^2 u_1^1$ and $b_\alpha^2 = -\rho\omega^2 u_\alpha^0$.

The global balances of forces and momentum acting on the section are obtained by integrating over the beam section S_b the scalar and vectorial balances. It defines $N\underline{a}_1$ the normal effort $N = \int_{S_b} \sigma_N ds$ and the shear force $\underline{T} = T_\alpha \underline{a}_\alpha = \int_{S_b} \underline{\sigma}_T ds$. The flexural momentum around y_2 and y_3 : $\underline{M} = M_\alpha \underline{a}_\alpha = \int_{S_b} \underline{y}_\alpha \sigma_N ds, \alpha = 2, 3$, and the torsional moment around x_1 : $M_1 = \int_{S_b} \underline{y} \wedge \underline{\sigma}_T ds$. The global equilibrium for normal and shear forces, flexural and torsional momentum, are written in the axial direction $\underline{a}_1$: $\frac{dN}{dx_1} = \int_{S_b} b_1 ds + \int_{\Gamma_b} f_1 d\gamma$; $\frac{d\underline{M}_1}{dx_1} = \int_\Gamma \underline{y} \wedge b_\alpha$, and in transverse directions $(\underline{a}_2, \underline{a}_3)$: $\frac{d\underline{T}}{dx_1} = (\int_{S_b} b_\alpha ds + \int_{\Gamma_b} f_\alpha d\gamma)\underline{a}_\alpha$; $\frac{d\underline{M}}{dx_1} - \underline{T} = \int_{S_b} b_1 \underline{y} ds + \int_{\Gamma_b} f_1 \underline{y} d\gamma$. To get the full description of the beam, it remains now to establish the constitutive laws.

A2. Beam model derived by asymptotic expansions

The purpose now is to derive the beam behavior through asymptotic approach. Each field of the problem (displacements, stresses, strains) is seeked in the form of an asymptotic expansions in power of ϵ_b. Due to (A.1), the balance equations and boundary conditions contain either terms in even (A.3) or odd (A.4) power of ϵ_b. Thus, it is enough to expand u_i in even powers of ϵ_b:

$$\tilde{u} = \sum_{i=0}^{\infty} \epsilon_b^{2i}(\epsilon_b u_1^{2i+1} \underline{a}_1 + u_\alpha^{2i} \underline{a}_\alpha), \ \text{with} \ \tilde{u}_1 = \sum_{i=0}^{\infty} \epsilon_b^{2i+1} u_1^{2i+1}, \ \text{and}$$
$$\tilde{u}_\alpha = \sum_{i=0}^{\infty} \epsilon_b^{2i} u_\alpha^{2i}$$

Thus, the reduced strain and stress tensors in the axis and in the cross-section (respectively tangential) are expanded in odd (respectively even) powers of ϵ_b:

$e_N = \epsilon_b^1 e_N^{(1)} + \epsilon_b^3 e_N^{(3)} + \dots$	$\sigma_N = \epsilon_b^{-1}\sigma_N^{(-1)} + \epsilon_b \sigma_N^{(1)} + \dots$
$\underline{e}_T = \epsilon_b^0 \underline{e}_T^{(0)} + \epsilon_b^2 \underline{e}_T^{(2)} + \dots$	$\underline{\sigma}_T = \epsilon_b^0 \underline{\sigma}_T^{(0)} + \epsilon_b^2 \underline{\sigma}_T^{(2)} + \dots$
$\underline{\underline{e}}_S = \epsilon_b^{-1} \underline{\underline{e}}_S^{(-1)} + \epsilon_b^1 \underline{\underline{e}}_S^{(1)} + \dots$	$\underline{\underline{\sigma}}_S = \epsilon_b^{-1} \underline{\underline{\sigma}}_S^{(-1)} + \epsilon_b^1 \underline{\underline{\sigma}}_S^{(1)} + \dots$

These expansions (A.5) are then introduced in balance Eqs. (A.3) and (A.4). This yields a series on the form $\sum_i \epsilon_b^i P^i = 0, \forall \epsilon_b << 1$, which leads to solve successively problems on the form $P^i = 0$. This resolution is performed solving alternatively problems in the axis and in the cross-section.

The first problem derived from (A.4) at order ϵ_b^{-2} expresses the in-plane equilibrium in the section of the tensor σ_S^{-1}, without external force:

$$\underline{div}_y(\underline{\underline{\sigma}}_S^{-1}) = 0 \ \text{ in } \ S_b; \qquad \underline{\underline{\sigma}}_S^{-1} = 2\mu \underline{\underline{e}}_S^{-1} + \lambda(tr(\underline{\underline{e}}_S^{-1}))I_S$$
$$\underline{\underline{\sigma}}_S^{-1}.\underline{n} = 0 \ \text{ on } \ \partial S_b$$

The resolution shows that the displacement u^0 at order 0 is a rigid body motion of the cross-section in its plane, *i.e.* translation U^0 and rotation $\Omega^{-1}\underline{a}_1$.

$$\underline{u}^0 = u_\alpha^0 \underline{a}_\alpha = U_\alpha^0(x_1)\underline{a}_\alpha + \Omega^{-1}\underline{a}_1 \wedge y$$

And consequently, $e_{Sy}(u^0) = 0$, $\underline{\underline{\sigma}}_S^{-1} = 0$ and $\sigma_N^{-1} = 0$. As the translation and the rotation are two independent mechanisms, we can consider that the rotation $\Omega^{-1} = 0$.

The second problem derived from (A.3) at order ϵ_b^{-1} expresses the axial balance of the section. Since $\sigma_N^{-1} = 0$, it reads:

$$div_y(\underline{\sigma}_T^0) = 0 \ \text{ in } \ S_b; \qquad \underline{\sigma}_T^0 = \mu(\partial_{y_\alpha} u_1^1 + \partial_{x_1} U_\alpha^0)a_\alpha$$
$$\underline{\sigma}_T^0.\underline{n} = 0 \ \text{ on } \ \partial S_b$$

which solution follows the Euler–Bernoulli kinematics $\underline{u}^1 = u_1^1 \underline{a}_1$ with $u_1^1 = -y_\alpha \partial_{x_1} U_\alpha^0 + U_1^1(x_1)$, so that $\underline{e}_T^0 = \underline{0}$ and $\underline{\sigma}_T^0 = \underline{0}$, and finally $\underline{\underline{e}}^0 = \underline{\underline{0}}$ and $\underline{\underline{\sigma}}^0 = \underline{\underline{0}}$.

The third problem derived from (A.4) at order ϵ_b^0 deals with the equilibrium in the section of the tensor $\underline{\underline{\sigma}}_S^1$,

$$\underline{div}_y(\underline{\underline{\sigma}}_S^1) = 0 \ \text{ in } \ S_b; \qquad \underline{\underline{\sigma}}_S^1 = 2\mu \underline{\underline{e}}_S^1 + \lambda(tr(\underline{\underline{e}}_S^1) + e_N^1)I_S$$
$$\underline{\underline{\sigma}}_S^1.\underline{n} = 0 \ \text{ on } \ \partial S_b$$

The resolution gives $\underline{\underline{e}}_S^1 = -\nu e_N^1 \underline{\underline{I}}$ and $\sigma_N^1 = E_b e_N^1$ where $e_N^1 = \partial_{x_1} u_1^1$ and $\underline{\underline{\sigma}}_S^0 = \underline{\underline{0}}$. Integrating σ_N^1 and $y_\alpha \sigma_N^1$ over the section S_b yields respectively the normal effort N and the constitutive law for flexural moments $\underline{M}$:

$$N = \int_{S_b} \sigma_N^1 ds = E_b S_b \frac{dU_1^1}{dx_1}; \qquad \underline{M} = \int_{S_b} \sigma_N^1 y_\alpha ds \underline{a}_\alpha = -E_b I_{b\alpha} \frac{d^2 U_\alpha^0}{dx_1^2}\underline{a}_\alpha$$

The fourth problem derived from (A.3) at order ϵ_b deals with the axial balance of $\underline{\sigma}_T^2$ in presence of a dynamic term and contact force on Γ:

$$\partial_{x_1}\sigma_N^1 + div_y(\underline{\sigma}_T^2) = -\rho\omega^2 u_1^1 \ \text{ in } \ S_b \qquad \underline{\sigma}_T^2 = \mu(\partial_{y_\alpha} u_1^3 + \partial_{x_1} U_\alpha^2)\underline{a}_\alpha$$
$$\underline{\sigma}_T^2.\underline{n} = \begin{cases} 0 \ \text{ on } \ \partial S_b - \Gamma_b \\ f_1 \ \text{ on } \ \Gamma_b \end{cases}$$

Integrating the axial balance over the section S_b leads to $\partial_{x_1}\int_{S_b}\sigma_N^1 + \int_{S_b} div_y(\underline{\sigma}_T^2) = -\rho\omega^2 \int_{S_b} u_1^1$. Furthermore, noting:

$$\int_{S_b} div_y(\underline{\sigma}_T^2) = \int_{\Gamma_b} \underline{\sigma}_T^2.n_{\Gamma_b} = \int_{\Gamma_b} f_1$$

with n_2 the component of the outgoing normal of the beam section, taking the value ± 1 on $\Gamma_b^\pm$, one obtains the axial balance along $\underline{a}_1$:

$$\partial_{x_1} N + \int_{\Gamma_b} f_1 = -\rho\omega^2 \int_{S_b} u_1^1$$

In a similar way, the momentum balance is obtained by multiplying the axial balance by y_α, then integrating over S_b yields

$$\partial_{x_1}\int_{S_b} y_\alpha \sigma_N^1 + \int_{S_b} y_\alpha div_y \underline{\sigma}_T^2 = -\rho_b S_b \omega^2 \int_{S_b} y_\alpha u_1^1$$

noting that

$$\int_{S_b} y_\alpha div_y(\underline{\sigma}_T^2) = \int_S div_y(y_\alpha \underline{\sigma}_T^2) - \int_{S_b} \underline{\sigma}_T^2 \underline{grad}_y(y_\alpha)$$

In addition, we have on one hand

$$\int_{S_b} div_y(y_\alpha \underline{\sigma}_T^2) = \int_{\Gamma_b} y_\alpha(\underline{\sigma}_T^2.\underline{a}_2) = \int_{\Gamma_b} y_\alpha f_1$$

and, on the other hand

$$\int_{S_b} \underline{\sigma}_T^2 \underline{grad}_y(y_\alpha) = \int_{S_b} \sigma_{T_{1\alpha}}^2 = \underline{T}_\alpha$$

We obtain the moment balance along $\underline{a}_\alpha$:

$$\partial_{x_1}\underline{M} + \int_{\Gamma_b} y_\alpha f_1 - \underline{T}_\alpha = -\rho\omega^2 \int_{S_b} \underline{y} u_1^1$$

The inertial term is specified further observing that

$$\int_{S_b} y_\alpha u_1^1 = \int_{S_b}\left(-y_\alpha y_\beta \frac{\partial U_\beta^0}{\partial x_1} + y_\alpha U_1^1(x_1)\right)$$
$$= -\frac{\partial U_\alpha^0}{\partial x_1}\int_{S_b} y_\alpha^2 = E_b I_{b\alpha}\frac{\partial U^0}{\partial x_1}$$

The fifth problem derived from (A.4) at order ϵ_b^2 deals with the equilibrium in the section of the tensor $\underline{\underline{\sigma}}_S^3$.

$$\partial_{x_1}\underline{\sigma}_T^2 + \underline{div}_y(\underline{\underline{\sigma}}_S^3) = -\rho_b\omega^2(U_\alpha \underline{a}_\alpha) \ \text{ in } \ S_b \quad \underline{\underline{\sigma}}_S^3.\underline{n} = 0 \ \text{ on } \ \partial S_b - \Gamma_b$$

Integrating this expression over S_b yields

$$\int_{S_b} \partial_{x_1}\underline{\sigma}_T^2 + \int_{S_b} \underline{div}_y(\underline{\underline{\sigma}}_S^3) = -\rho_b S_b \omega^2 U_\alpha \underline{a}_\alpha$$

On one hand, the first left hand side term is $\partial_{x_1}\underline{T}$, and on the other hand:

$$\int_{S_b} div_y(\underline{\underline{\sigma}}_S^3) = \int_{\Gamma_b} \underline{\underline{\sigma}}_S^3 n_\Gamma = \int_{\Gamma_b} f_\alpha \underline{a}_\alpha$$

The term b_α accounting for transverse dynamic appears in the global shear effort in the form:

$$\partial_{x_1}\underline{T} = -\rho_b S_b \omega^2 U_\alpha^0 \underline{a}_\alpha - \int_{\Gamma_b} f_\alpha \underline{a}_\alpha$$

To sum-up, the global balance equation for compression, and the bending moment, moment balance along $\underline{a}_\alpha$, and the global shear effort are:

$$\begin{cases} \partial_{x_1} N + \int_{\Gamma_b} f_1 = -\rho\omega^2 \int_{S_b} u_1^1 \\ N = E_b S_b \dfrac{dU_1^1}{dx_1} \end{cases} ; \quad \begin{cases} \partial_{x_1} T_\alpha + \int_{\Gamma_b} f_\alpha \underline{a}_\alpha \\ \qquad = -\rho_b S_b \omega^2 U_\alpha^0(x_1) \\ \partial_{x_1}\underline{M} + \int_{\Gamma_b} y_\alpha f_1 - T_\alpha = 0 \\ \underline{M} = -E_b I_b \dfrac{d^2 U_\alpha^0}{dx_1^2} \end{cases} \tag{A.6}$$

References

Altenbach, J., Altenbach, H., Eremeyev, V.A., 2010. On generalized Cosserat-type theories of plates and shells: a short review and bibliography. Arch. Appl. Mech. 80 (1), 73–92. doi:10.1007/s00419-009-0365-3.

Auriault, J.-L., Bonnet, G., 1985. Dynamique des composites élastiques périodiques. Arch. Mech. 37 (4–5), 269–284.

Auriault, J.-L., Boutin, C., 2012. Long wavelength inner-resonance cut-off frequencies in elastic composite materials. Int. J. Solids Struct. 49 (2324), 3269–3281. doi:10.1016/j.ijsolstr.2012.07.002.

Auriault, J.-L., Boutin, C., Geindreau, C., 2009. Homogenization of coupled phenomena in heterogenous media (ISTE), first ed. Wiley-ISTE.

Berdichevsky, V.L., 2010. An asymptotic theory of sandwich plates. Int. J. Eng. Sci. 48 (3), 383–404. doi:10.1016/j.ijengsci.2009.09.001.

Berthaut, J., Ichchou, M., Jezequel, L., 2005. K-Space identification of apparent structural behaviour. J. Sound Vib. 280 (35), 1125–1131. doi:10.1016/j.jsv.2004.02.044.

Boutin, C., 1996. Microstructural effects in elastic composites. Int. J. Solids Struct. 33 (7), 1023–1051. doi:10.1016/0020-7683(95)00089-5.

Caillerie, D., 1984. Thin elastic and periodic plates. Math. Methods Appl. Sci. 6 (1), 159–191. doi:10.1002/mma.1670060112.

Chesnais, C., Boutin, C., Hans, S., 2012. Effects of the local resonance on the wave propagation in periodic frame structures: generalized newtonian mechanics. J. Acoust. Soc. Am. 132 (4), 2873–2886. doi:10.1121/1.4744975.

Ciarlet, P., 1997. Theory of plates. Mathematical Elasticity. Elsevier Science.

Droz, C., Lain, J.-P., Ichchou, M., Inquiété, G., 2014. A reduced formulation for the free-wave propagation analysis in composite structures. Compos. Struct. 113, 134–144. doi:10.1016/j.compstruct.2014.03.017.

Fahy, F., Lindqvist, E., 1976. Wave propagation in damped, stiffened structures characteristic of ship construction. J. Sound Vib. 45 (1), 115–138. doi:10.1016/0022-460X(76)90671-4.

Hussein, M.I., Leamy, M.J., Ruzzene, M., 2014. Dynamics of phononic materials and structures: historical origins, recent progress, and future outlook. Appl. Mech. Rev. 66 (4), 040802. doi:10.1115/1.4026911.

Ichchou, M., Akrout, S., Mencik, J.-M., 2007. Guided waves group and energy velocities via finite elements. J. Sound Vib. 305 (4), 931–944. doi:10.1016/j.jsv.2007.05.007.

Ichchou, M., Berthaut, J., Collet, M., 2008. Multi-mode wave propagation in ribbed plates: part I, wavenumber-space characteristics. Int. J. Solids Struct. 45 (5), 1179–1195. doi:10.1016/j.ijsolstr.2007.09.032.

Ichchou, M., Berthaut, J., Collet, M., 2008. Multi-mode wave propagation in ribbed plates. part ii: predictions and comparisons. Int. J. Solids Struct. 45 (5), 1196–1216. doi:10.1016/j.ijsolstr.2007.08.020.

Kalamkarov, A., Andrianov, I., Danishevs'kyy, V., 2009. Asymptotic homogenization of composite materials and structures. Appl. Mech. Rev. 62 (3), 030802–1–030802–20. doi:10.1115/1.3090830.

Kohn, R.V., Vogelius, M., 1984. A new model for thin plates with rapidly varying thickness. Int. J. Solids Struct. 20 (4), 333–350. doi:10.1016/0020-7683(84)90044-1.

Lewiński, T., Telega, J., 2000. Plates, laminates, and shells: asymptotic analysis and homogenization. Series on Advances in Mathematics for Applied Sciences. World Scientific.

Mace, B.R., Duhamel, D., Brennan, M.J., Hinke, L., 2005. Finite element prediction of wave motion in structural waveguides. J. Acoust. Soc. Am. 117 (5), 2835–2843. doi:10.1121/1.1887126.

McDaniel, J.G., Shepard, W.S., 2000. Estimation of structural wave numbers from spatially sparse response measurements. J. Acoust. Soc. Am. 108 (4), 1674–1682. doi:10.1121/1.1310668.

Mead, D., 1973. A general theory of harmonic wave propagation in linear periodic systems with multiple coupling. J. Sound Vib. 27 (2), 235–260. doi:10.1016/0022-460X(73)90064-3.

Mejdi, A., Atalla, N., 2010. Dynamic and acoustic response of bidirectionally stiffened plates with eccentric stiffeners subject to airborne and structure-borne excitations. J. Sound Vib. 329 (21), 4422–4439. doi:10.1016/j.jsv.2010.04.007.

Sanchez-Palencia, E., 1980. Non-homogeneous media and vibration theory. Lecture Notes in Physics, spi ed. Springer.

Soubestre, J., Boutin, C., 2012. Non-local dynamic behavior of linear fiber reinforced materials. Mech. Mater. 55 (0), 16–32. doi:10.1016/j.mechmat.2012.06.005.

Trabucho, L., Viaño, J., 1996. Mathematical modelling of rods. In: Finite Element Methods (Part 2), Numerical Methods for Solids (Part 2). In: Handbook of Numerical Analysis, 4. Elsevier, pp. 487–974. doi:10.1016/S1570-8659(96)80006-8.

Trévisan, B., Ege, K., Laulagnet, B., 2016. Vibroacoustics of orthotropic plates ribbed in both directions: application to stiffened rectangular wood panels. J. Acoust. Soc. Am. 139 (1), 227–246. doi:10.1121/1.4939706.

Ungar, E.E., 1961. Transmission of plate flexural waves through reinforcing beams; dynamic stress concentrations. J. Acoust. Soc. Am. 33 (5), 633–639. doi:10.1121/1.1908748.

Varanasi, S., Bolton, J.S., Siegmund, T.H., Cipra, R.J., 2013. The low frequency performance of metamaterial barriers based on cellular structures. Appl. Acoust. 74 (4), 485–495. doi:10.1016/j.apacoust.2012.09.008.

Viverge, K., Boutin, C., Sallet, F., 2016. Model of highly contrasted plates versus experiments on laminated glass. Int. J. Solids Struct. 102–103, 238–258. doi:10.1016/j.ijsolstr.2016.09.035.

Waki, Y., Mace, B., Brennan, M., 2009. Numerical issues concerning the wave and finite element method for free and forced vibrations of waveguides. J. Sound Vib. 327 (12), 92–108. doi:10.1016/j.jsv.2009.06.005.

Zhou, C.W., Lainé, J.P., Ichchou, M.N., Zine, A.M., 2015. Wave finite element method based on reduced model for one-dimensional periodic structures. Int. J. Appl. Mech. 07 (02), 1550018. doi:10.1142/S1758825115500180.